Approaches of Satellite Remote Sensing for the Assessment of Above-Ground Biomass across Tropical Forests: Pan-tropical to National Scales

Sawaid Abbas [1], **Man Sing Wong** [1,2,*], **Jin Wu** [3], **Naeem Shahzad** [1] and **Syed Muhammad Irteza** [1]

[1] Department of Land Surveying and Geo-Informatics, The Hong Kong Polytechnic University, Hung Hom, Hong Kong, China; sawaid.abbas@connect.polyu.hk (S.A.); naeem.shahzad@connect.polyu.hk (N.S.); syed-m.irteza@connect.polyu.hk (S.M.I.)

[2] Research Institute for Sustainable Urban Development, The Hong Kong Polytechnic University, Hung Hom, Hong Kong, China

[3] School of Biological Sciences, The University of Hong Kong, Pokfulam, Hong Kong, China; jinwu@hku.hk

* Correspondence: lswong@polyu.edu.hk

check for
updates

Abstract: Tropical forests are acknowledged for providing important ecosystem services and are renowned as "the lungs of the planet Earth" due to their role in the exchange of gasses—particularly inhaling CO_2 and breathing out O_2—within the atmosphere. Overall, the forests provide 50% of the total plant biomass of the Earth, which accounts for 450–650 PgC globally. Understanding and accurate estimates of tropical forest biomass stocks are imperative in ascertaining the contribution of the tropical forests in global carbon dynamics. This article provides a review of remote-sensing-based approaches for the assessment of above-ground biomass (AGB) across the tropical forests (global to national scales), summarizes the current estimate of pan-tropical AGB, and discusses major advancements in remote-sensing-based approaches for AGB mapping. The review is based on the journal papers, books and internet resources during the 1980s to 2020. Over the past 10 years, a myriad of research has been carried out to develop methods of estimating AGB by integrating different remote sensing datasets at varying spatial scales. Relationships of biomass with canopy height and other structural attributes have developed a new paradigm of pan-tropical or global AGB estimation from space-borne satellite remote sensing. Uncertainties in mapping tropical forest cover and/or forest cover change are related to spatial resolution; definition adapted for 'forest' classification; the frequency of available images; cloud covers; time steps used to map forest cover change and post-deforestation land cover land use (LCLU)-type mapping. The integration of products derived from recent Synthetic Aperture Radar (SAR) and Light Detection and Ranging (LiDAR) satellite missions with conventional optical satellite images has strong potential to overcome most of these uncertainties for recent or future biomass estimates. However, it will remain a challenging task to map reference biomass stock in the 1980s and 1990s and consequently to accurately quantify the loss or gain in forest cover over the periods. Aside from these limitations, the estimation of biomass and carbon balance can be enhanced by taking account of post-deforestation forest recovery and LCLU type; land-use history; diversity of forest being recovered; variations in physical attributes of plants (e.g., tree height; diameter; and canopy spread); environmental constraints; abundance and mortalities of trees; and the age of secondary forests. New methods should consider peak carbon sink time while developing carbon sequestration models for intact or old-growth tropical forests as well as the carbon sequestration capacity of recovering forest with varying levels of floristic diversity.

Keywords: above-ground biomass; remote sensing; tropical forest; pan-tropics; carbon stock; biomass

1. Introduction

The loss and degradation of the world's forests are major contributors to biodiversity loss and climate change [1]. Forests occupy the largest plant community on the land surface of the Earth, sequestrate most of the atmospheric carbon [2], are an overall sink of −2.1 Gt CO_2 per year [3], and, hence, play a pivotal role in the global carbon cycle [4]. Tropical ecosystems span over ~ 33% of the global land area [5] and are the major contributor of global CO_2 sink. The tropical forests occupy 45% (1.827 billion ha) of the total global forests (4.06 billion ha) [6]. These forests contribute 56% (1.4 billion metric tons) of the terrestrial absorption of atmospheric CO_2 [7] at an annual rate of 1.3 PgC [8]. Tropical forests are also acknowledged for providing important ecosystem services, including biomass production, carbon stock, carbon sequestration (or fluxes) and global and regional climate patterns [9]. Collectively, tropical forests provide 50% of the total plant biomass of the Earth [10], and are renowned as "the lungs of the planet Earth" due to their role in the exchange of gasses, particularly inhaling CO_2 and breathing out O_2, within the atmosphere [11].

Tropical forests are dynamic ecosystems that undergo successional changes [12,13], natural disturbances, deforestation and land degradation [14]. Recent evidence from a detailed time series of satellite images indicates a 62% increase in deforestation in the humid tropics from the 1990s to the 2000s [15]. A broad outline prediction of the future of tropical forest indicates extensive agricultural encroachment into the old-growth forest due to an expected 2 billion increase in the population of tropical countries over the next few decades [16]. However, the recent Forest Recourses Assessments (FRA) by the Food and Agriculture Organization (FAO) [6], reported a 32% reduction in an annual deforestation rate of tropical forests from the 1990s to the latter half of the 2020s. On the other hand, secondary succession has regained 15% of the area deforested during the 1990s, as a result of millions of hectares of the tropical landscape being abandoned following massive deforestation and large-scale agricultural activities [17]. Knowledge of accurate and up-to-date forest inventories, recovery rates and variation in regrowth rates across time and space is mandatory in facilitating well-informed management, and in understanding biomass and carbon sequestration potential of these dynamic ecosystems to mitigate future climate change impacts reducing the uncertainties in estimating global carbon flux.

However, it is difficult to ascertain structural characteristics of these difficult-to-access ecosystems through conventional field-based inventories, as the tropical forests are composed of a variety of species with high structural and biological diversity varying along with spatial and temporal scales [18]. Field-based carbon stock inventories of the huge tropical forest area (approximately 18 million km^2) are logistically challenging, time demanding and difficult to repeat over time to monitor the growth. Existing long-term and short-term field plots in the tropical forest provide invaluable information about forest functions and attributes, but are too small in terms of numbers to fully represent the dynamics of tropical systems and carbon stocks [18].

Rapidly developing space-borne and air-borne remote sensing technologies and tools are increasingly used to obtain quick, reliable and consistent information over large areas [19], complementing less frequent and spatially limited field inventories, to understand tropical forest ecosystem function, structure, and productivity, and to record changes in the forests' attributes (e.g., leaf area structure, basal area, stem volume, and basal-area weighted mean diameter and basal-area weighted mean height) at varying spatial and temporal scales [20]. Estimates of above-ground biomass (AGB) of forests are obtained from different methodologies and variety of sources such as field measurements, national forest inventories, administrative-level statistics, model outputs and regional satellite products [21]. FAO's FRA [22] is the sole global dataset which provides carbon stock aggregated at the country-level from 1990 to 2015, covering all 229 countries and territories of the world [3]. Complementary to this is an additional repository of a database on forest carbon dynamics by the United Nations Framework Convention on Climate Change (UNFCCC), which contains data submitted by its parties.

Remote sensing cannot provide direct measurements of biomass [23], although the role of remote sensing is pivotal for accurate and up-to-date measurement of forest structure to estimate carbon stocks and fluxes of the forests. Field-inventory-based methods of biomass estimation are time-consuming, suffer from the low sample size, are inconsistent across space and do not indicate actual estimation of the AGB in a landscape [24–26]. However, these methods are important and have played a significant role in developing allometric equations for biomass estimation. Remote sensing can help in resolving the restraints of the conventional AGB measurement methods, especially in inaccessible tropical forests, by providing cost-effective, repeatable, spatially contiguous and explicit observations [27,28]. Nonetheless, remote-sensing-based methods are in transition to become independent and solicit methods of AGB modelling. Therefore, current conventional measurements (biophysical characteristics of vegetation) are being integrated with various remote sensing datasets to quantify and monitor biomass stocks across a wide range of spatial and temporal scales [9,20,29–31]. For example, vital structural attributes of forests or trees to develop allometric models of biomass estimations can be retrieved from laser scanners [32–35]. Thus, pan-tropical or sampling-based remote sensing data can be acquired to complement the destructive field-based inventories and reduced efforts from conventional field surveys, for estimating tree attributes to develop allometric models in an inaccessible area or expand the existing tree inventories to all tropical forest types. Thus, remote-sensing-based biomass measurements are derived by statistical and/or machine learning-based integration of tree/stand/plot level allometric models with spatially contiguous forest extent and structural information derived from remote sensing data [18].

In this paper, we reviewed the remote sensing methods applied to determine the AGB in the tropical forests and future biomass measurement missions. This review focuses on the large-scale studies at the pan-tropical, regional or national level. Local scales studies are not incorporated in the analysis and discussion, but a brief overview is included whenever it was necessary to explain a relevant method or advancement. The scope of this paper covers a wide range of relevant sources—journal papers, books and internet resources between the year 1980 and 2020 with the keywords of Tropical Forest, Remote Sensing, Biomass, Above-Ground Biomass, Carbon Stock, Forest Change, Tropical Degradation and Tropical Deforestation in Web of Science, Scopus and Google Scholar (accessed in April 2020). The keywords were used with the search operator of 'AND', with the following combinations, 'tropical AND forest', 'remote sensing AND biomass', 'above-ground biomass AND carbon stock', 'forest change', 'degradation AND deforestation'. Another filter 'tropical AND remote sensing AND biomass' was applied to narrow down the search results. Besides, considering the importance of land cover products in the AGB estimation, we provided a brief overview of the global or pan-tropical land cover products used in the AGB estimation studies or have potential to be used in near future. Similarly, other modalities of remote sensing encompassing forest compositions and structural attributes are included to provide a broader perspective of contributing factors. We found around 200 most relevant papers/articles with the mentioned keywords and found increasing interest among researchers to study AGB for tropical forests in terms of publications over the last 40 years (Figure 1). The higher number of published documents in the last decade may be related to the increased interest of the scientific community in studying the impact of climatic variations on tropical forests functioning as well as new satellite missions with enhanced capacities of large-scale mapping. We observed that the number of publications is increased by three-folds over the last decade. The trend in increasing publications will be accelerated in the next 10–15 years with the launch of biomass-specific satellite missions. The review is intended to summarize major advancements in remote-sensing-based studies of pan-tropical AGB mapping. It is also supplemented with an appendix consisting of a list of abbreviations used in the study (Table A1), a brief description of relevant AGB mapping studies in the tropical forests (Table A2), and salient features of frequently used passive (Table A3) and active (Table A4) satellite remote sensing missions.
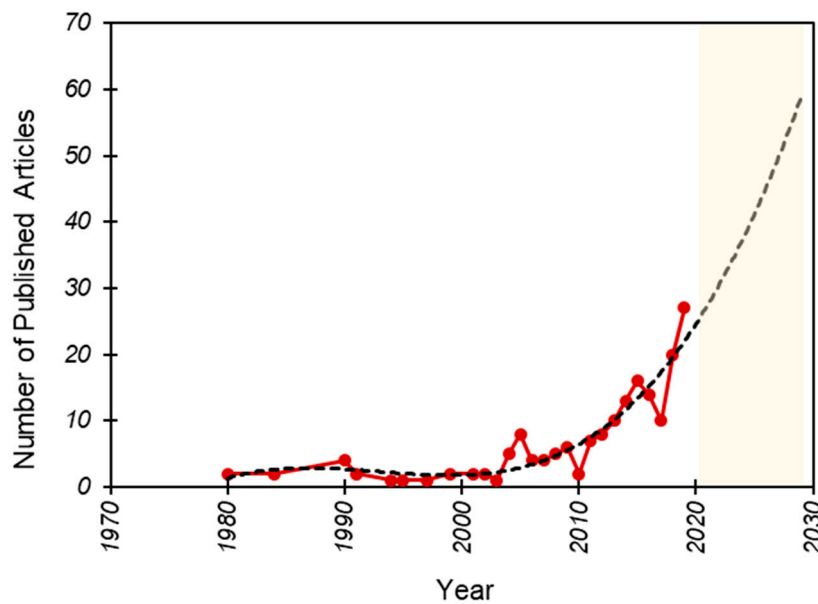
Figure 1. The number of documents on above-ground biomass (AGB) of tropical forests published in the last 40 years, and expected increase in the relevant publication in the coming decade, the dotted line indicates polynomial fit.

2. Field Inventories and Remote Sensing for Biomass Estimation

Estimates of the AGB of forests are obtained from different methodologies and a variety of sources, such as field measurements, national forest inventories, administrative-level statistics, model outputs and regional satellite products [21]. The conventional methods in obtaining biomass are carried by developing allometric equations, biomass expansion factors (BEF) or conversion factors which are based on regression between tree biomass and tree attributes such as height, diameter, wood density and leaf biomass at a sampled location. These models are extrapolated using statistical or machine learning approaches to estimate total biomass stock across the landscapes of interest [36].

AGB is referred to total living biomass, including trees, shrubs and vines above the ground. It is measured in units of tons of carbon per unit area by oven drying the total mass of organic living plant matter [37]. The reference or direct biomass is measured by the cutting down of selected trees (including stump, stem, twig, branches, bark and foliage) belonging to different species, dried in an oven and then their weight is measured in a laboratory. This is a destructive and unsustainable approach, but is the most accurate method of biomass estimation. Then, the reference biomass is used to develop species-specific allometric models by regressing it as a function of physical attributes of the trees such as diameter at breast height (DBH), tree height, canopy spread and wood density [38].

Once the allometric equations are derived, nondestructive methods can be followed to determine AGB. In situ nondestructive estimation of AGB is carried by measuring height and DBH in randomly dispersed field sample plots. Establishing 50 forest inventory plots of 1 ha (100 m by 100 m) is a recommended practice for assessing biomass and stem density in tropical forests [39]. FAO has established protocols in assessing AGB using field-based inventories in the 'Manual for Building Tree Volume and Biomass Allometric Equations' [40]. These estimations are important to understand forest structure, productivity, carbon fluxes, carbon sequestration, and condition of tree site [41]. However, measuring height and DBH across the landscape could be time-consuming, costly and difficult to repeat. Errors in height and DBH measurements can also induce uncertainties in biomass estimation from allometric models [42]. Besides, caution must be taken while extrapolating biomass from allometric models across a landscape as the growing conditions can vary with land-use history, successional stage of forests, environmental and climatic constraints [43,44].

Remote-sensing-based products play a pivotal role in upscaling and parameterization of field/plot level inventories of forest structure, ecosystem processes and models. The basic idea of remote-sensing-based upscaling revolves around association of field/plot based attributes with land cover characteristics or forest structure or spectral response and then extrapolation of the relationship across the extent of the landscape [45]. Xiao et al. [46] documented the advances and milestones achieved in biomass estimations from remote sensing since the late 1970s. A brief description of relevant AGB mapping studies in tropical forests is provided in the Table A2 (please see Appendix A). Precise synopsis of several procedures, algorithms and methods of modelling and estimating biomass from a variety of remote sensing data is presented by Lu et al. [44]. They highlighted the importance of multi-sensor data integration in biomass modelling studies.

In a broader perspective, both active and passive remote sensing sensors are valuable for carbon stock mapping, but active sensors, such as Synthetic Aperture Radar (SAR) and Light Detection and Ranging (LiDAR), have enormous potential for more accurate and useful proxies for forest biomass inventories than the passive sensors [23]. The rise of advanced remote sensing instruments with high spatial and temporal resolution had advanced the monitoring of biomass and carbon flux inventories at global, regional and local scales [47]. The ability of airborne LiDAR observation to penetrate the upper canopy layer produces highly accurate AGB estimates in multi-layered tropical forests. The mapping accuracy increases further when the LiDAR data are combined with high-spatial-resolution multispectral or hyperspectral images.

The prime focus of remote-sensing-based carbon stock assessment studies is largely related to the AGB which accounts for 450–650 PgC globally [48]. Likewise, carbon sequestration studies emphasized on the balance between net primary productivity (NPP), ~60 PgC per year globally [48], and losses, ~3.5 PgC per year [49], due to anthropogenic (e.g., deforestation, degradation, land cover land use (LCLU) change) and natural influences (e.g., fire) on vegetation and vegetation processes [50]. Remote sensing facilitates to quantify and understand the role of Earth's biosphere in governing the flux rates of atmospheric CO_2 concentration by monitoring NPP and Net Ecosystem Production (NEP) [47]. Remote sensing provides promising products (such as NPP, Gross Primary Production (GPP), Sun-Induced Chlorophyll Fluorescence (SIF)) in process-based ecosystem models for spatio-temporal assimilation and quantification of carbon fluxes on regional and global scales [47,51].

3. Mapping of Land Cover and Physiological or Structural Variables

The mapping and quantification of biomass and carbon sequestration are important in terms of large-scale LCLU changes and policy development of national and regional REDD+ (Reducing Emissions from Deforestation and Forest Degradation, and the role of conservation, sustainable management of forests and enhancement of forest carbon stocks in developing countries) initiatives in tropical forest ecosystems [50]. Therefore, the role of remote sensing is important for the accurate and up-to-date measurement of land surface characteristics to estimate carbon stocks and fluxes of the forests, despite the fact that remote sensing cannot provide direct measurements of biomass [23]. However, it is a powerful tool to upscale field/plot-based inventories to the landscape/regional/continental-level understanding [45]. It provides numerous valuable inputs, such as LCLU maps, Leaf Area Index (LAI), phenology, stand age, forest structure, and an estimate of the net and gross primary productivity, to empirical and processed oriented models of forest biomass and carbon flux measurements, productivity, structure and composition [18,45]. The above-mentioned attributes for forest biomass, carbon flux measurements and ecosystem processes are extracted by applying various methods on an array of remote sensing data recorded by instruments that differ by platform (spaceborne and airborne), electromagnetic waveband (e.g., multispectral, hyperspectral), active (e.g., SAR and LiDAR) and passive (spectrometer) systems, resolution (spatial, temporal and spectral) and area coverage (global or regional) (Figure 2) [47,52].
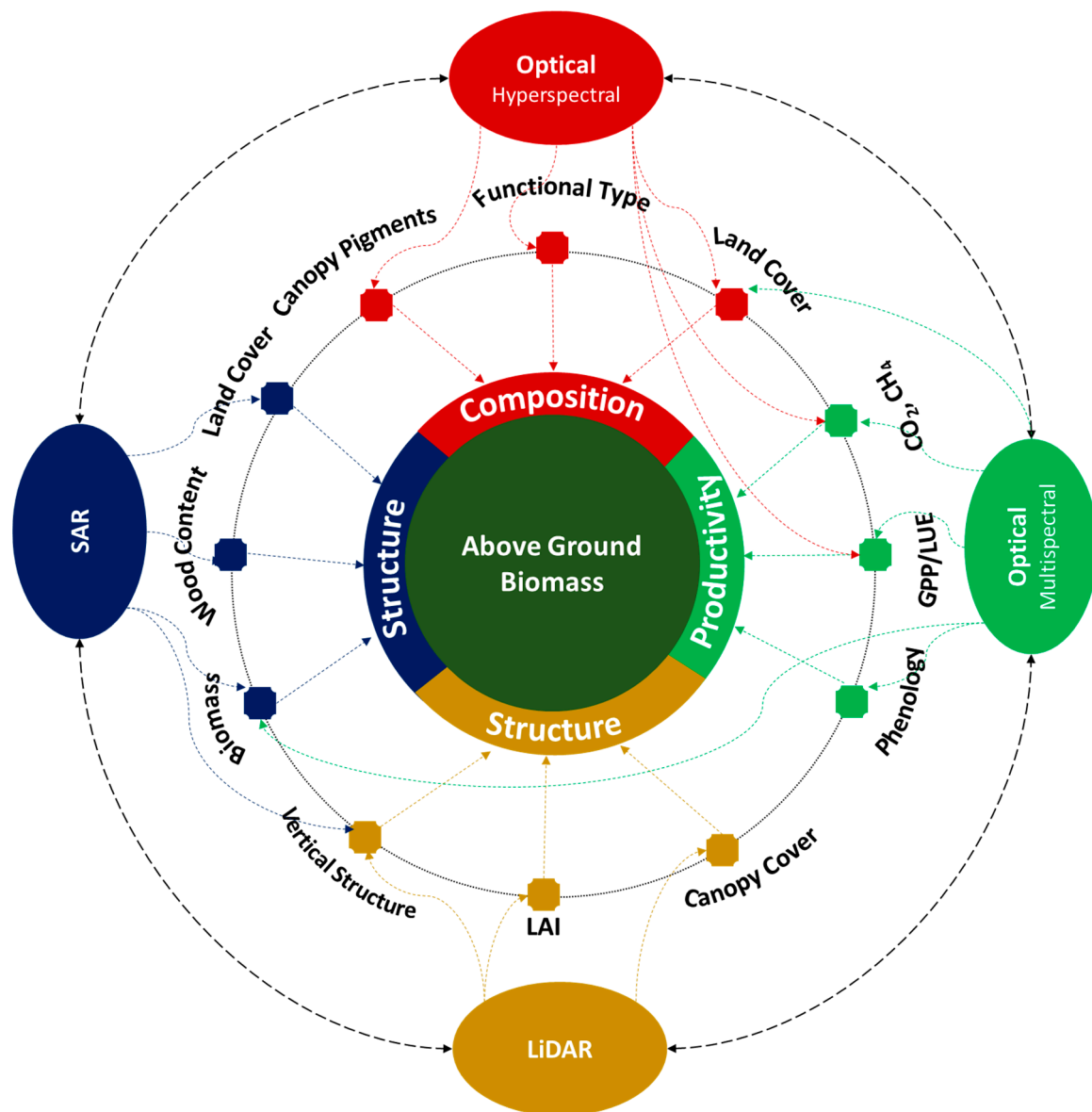
Figure 2. Remote sensing approaches for mapping biomass by extracting various parameters indicating productivity, composition and structure of forest from passive or optical (multispectral and hyperspectral) and active (Light Detection and Ranging (LiDAR) and Synthetic Aperture Radar (SAR)) sensors.

3.1. Land Cover Products

Land Cover (LC) map is one of the primary inputs for implementing carbon stock assessment models across a wide range of spatial coverage [53,54]. Figure 3 shows the distribution of forests across the tropics derived from the recently released global LC product by the European Space Agency (ESA) under the Copernicus Global Land Service (CGLS) [55]. Changes in LC dynamically interact with the regional and global carbon cycle and influence AGB [56]. The changes in physiology, functional attributes and allometry of different vegetation types varies across space and have a different environmental response. The LC maps help to extrapolate plot-level measurements to landscape-level estimates of a generalized carbon budget. The primary limitation of the LC map-based estimation of the biomass is the generalizability issue associated with the spatial resolution, i.e., mixing of different vegetation forms, as well as at major classes of the vegetation type, e.g., forest, which may vary in structural and productivity characteristics across the landscape and grain unit.

Global-scale LC classification started with the advent of daily Advanced Very High Resolution Radiometer (AVHRR) datasets (4-km spatial resolution) in the early 1980s [57], which were later enhanced by using phenological and seasonal attributes derived from bi-monthly vegetation indices from the reprocessed AVHRR data at an 8-km spatial resolution in the framework of the Global Inventory Monitoring and Modeling System (GIMMS) project [58]. A Moderate-Resolution Imaging Spectroradiometer (MODIS)-based global forest condition map is produced by the Atlas of Forest Landscape Restoration Opportunities by Global Restoration Initiative jointly produced by collaboration among the World Resource Institute (WRI), University of Maryland (UMD) and International Union for Conservation of Nature (IUCN) [59]. The atlas aimed at providing the spatial extent of current forest coverage and forest degradation restoration opportunities at a 1-km spatial resolution. These maps are derived from 250 m global mosaics of MODIS for 2000 to 2009 and MODIS vegetation continuous field (VCF) [60]. However, the maps may not be good for local scenarios due to averaging at a 1-km spatial unit. Detailed mapping of forest AGB estimation has been accelerated since 2008 after the implementation of open access policy of the Landsat images [61]. Several studies have been conducted to map land cover attributes on the local, regional and global scales. An online portal, Global Forest Watch (GFW), provides [62] quantitative estimates of the global forest and land cover coverage and change statistics by using various mapping products, such as tropical forest cover change alerts [63] and global tree cover changes, with different spatial resolutions ranging from 30 to 500 m, temporal coverages between 2001 and 2019 and update frequencies (daily, weekly, monthly, annual, 12 and 18 years) [63–68]. Figure 3 represents the spatial distribution of tropical forests extracted from the Copernicus Global Land Service–Land Cover 100 (CGLS-LC100) produced at a 10 m spatial resolution by the ESA under the Climate Change Initiative (CCI) [69,70]. Recently, a global habitat map of terrestrial ecosystems, based on the IUCN habitat classification scheme, has been developed by integrating satellite-derived LCLU maps (CGLS-LC100) with climate, topography and other ancillary datasets [71]. Details of other studies and datasets of forest cover extent, losses, and gains at the pan-tropical or global level are given in Tables 1 and 2.

Global Land Analysis and Discovery (GLAD) is a robust humid tropical rainforest alert system developed by using Landsat data [63]. The data are produced with high accuracy, but limitation arises due to continuous cloud cover over the tropical regions and lack of ground validation data. Inaccuracies induced by the presence of cloud cover over the region can be reduced by incorporating SAR data [72]. Moreover, the accuracy of the alert system can be increased by using spectral unmixing methods [73]. Similar limitation of cloud cover presence was found in a Terra-i real-time monitoring system by the International Center for Tropical Agriculture (CIAT) [66] and CGLS-LC100 by the ESA [69,70], which reduces the accuracy of the products in tropical regions. The CGLS-LC100 is a recently released product and has not been used in estimating tropical AGB, though it has strong potential for pan-tropical forest cover change and biomass models due to its higher temporal frequency. The MODIS based Atlas of Forest Landscape and Restoration Opportunities [59] product estimated that more than two billion hectares of land globally have a potential for monitoring restoration of forests mostly in temperate and tropical landscapes. Use of this product requires cautions as the product is produced at a coarse spatial resolution (1 km), lower in accuracy, lacks data for field validation and land-use dynamics. This global map provides no information for policymaker regarding restoration intervention efforts that are needed for regional- or local-scale restoration projects [74]. Forest Monitoring for Action (FORMA) [64], a monthly product, has the limitation of coarse resolution 500 m but the main advantage of this product lies in its geographic focus over the humid tropics. FORMA250 [65], an updated version of the FORMA, improves the previous model by providing daily updates at a 250 m spatial resolution and extended geographic coverage across the tropics. The FORMA products are ingested in the Google Earth Engine (GEE), making them more resourceful for cloud bases biomass mapping studies. The Global Mangrove Watch (GMW) [75] integrates the Phased Array type L-band Synthetic Aperture Radar (PALSAR) and Landsat data to understand mangroves cover dynamics with a minimum mapping unit (MMU) of 1 ha. The 1 ha MMU induces uncertainties

while assessing smaller vegetated areas as well as a disturbance occurring on a finer scale. The 34° off-nadir angle of PALSAR is too high for the detection of sparsely forested areas, which results in an underestimation of the total areas covered with forests [76]. Mapping accuracies in most of the studies involving Landsat data are affected by cloud cover and Scan Line Corrector (SLC) error of the Enhanced Thematic Mapper Plus (ETM+) sensor onboard Landsat-7. Statistical errors in different methodologies adopted by different forest mapping techniques can increase the discrepancies in land cover global products hence caution should be taken while using these datasets for local or regional policies.

Apart from land cover mapping products, the focus of global ecological assessment from remote sensing has shifted towards estimating functional traits such as Fraction of Vegetation Cover (FVC) and Tree Density [67,77], LAI, and Fractionally Absorbed Prosthetically Active Radiation (FAPAR) [78]. On a finer scale of plant functional traits such as chlorophyll concentration, carbon-nitrogen ratio, and SIF, estimation is commonly carried through high spectra resolution and hyperspectral remote sensing techniques. However, it remains challenging to transform these leaf-level processes to canopy and landscape-level processes which could be strongly influenced by canopy structure, branches, trunks, leaf area and canopy shadows [79–81].

Figure 3. Forest cover map derived from the Copernicus Global Land Service–Land Cover 100 (CGLS-LC100) [55].

Table 1. Global and/or pan-tropical land cover products of general structural characteristics of vegetation.

Program/Data Provider/ Product Name	Coverage	Satellite/ Sensor	Spatial Resolution	Year	Attributes	Reference
Global Land Analysis and Discovery (GLAD)	Humid Tropics	Landsat	30 m	2012–present	Tropical Deforestation	[63]
World Resources Institute (WRI)/FORMA	Humid Tropics	MODIS	500 m	2006–2015 Monthly	Tree Cover Loss	[64]
WRI/FORMA250	Pan-Tropics	MODIS	250 m	2012–present Daily	Forest Loss	[65]
CIAT/Terra-i	Pan-Tropics	MODIS/ TRMM	250 m	2012–present Monthly	Deforestation Hotspots	[66]
GLAD /NASA/UMD/ USGS/Google	Global	Landsat	30 m	2001–2018 Yearly	Tree Cover, Gain and Loss	[67]
Global Land Analysis and Discovery (GLAD)	Pan-Tropics	Landsat	30 m	2001	Tropical Primary Forest	[68]
Greenpeace, GLCF, UMD, WRI	Global	Landsat	30 m	2000, 2013, and 2016	Intact Forest Landscapes (IFL)	[82,83]
CGLS – Land Cover 100 (CGLS-LC100)/ESA	Global	PROBA-V Sentinel	100 m	2015–present	Land Cover Characteristics	[69,70]
GlobeLand30/ NASG	Global	Landsat	30 m	2000–2010	Land Cover Map and Changes	[84]
JAXA	Global	ALOS-PALSAR	25 m	2007–2015	Forest Maps	[76]

3.2. Physiological Variables

Specific modelling of structural and physiological changes in vegetation also serves as an important input parameter for biomass models, which can be substituted by adding leaf structure variables measured from remote sensing datasets and associated environmental and climate variables. Therefore, to avoid discrete LCLU classes, scientists have made efforts in developing alternative physiological variables, such as vegetation continuous field [85], life form [86], leaf type [59], phenology [51,87], and leaf longevity [78]. For example, a global product of MODIS-based VCF is produced at a 250 m resolution using an automated algorithm [88]. This product provides a percentage of tree cover, ranging from 0 to 100%, in a pixel and it is available at National Aeronautics and Space Administration (NASA)'s Land Processes Distributed Active Archive Center (LPDAAC). Sexton et al. [89] rescaled the MODIS 250 m VCF product by using Landsat and LiDAR-based data to produce a high-resolution global VCF at a 30 m resolution. VCF tree cover products have been widely used for biomass mapping across the tropics and globe [90–93]. For example, VCF is used to develop the baseline map of carbon emission from deforestation and degradation in the tropical area at a spatial resolution of 18.5 km [92]. The study found 0.81 PgC emissions from 2000 to 2005 due to forest cover loss across the tropics. Another study estimated mean annual changes in carbon stock due to tropical deforestation and regeneration during the 1980s and 1990s [93], using VCF derived from National Oceanic and Atmospheric Administration (NOAA)-AVHRR data. This study reported a 10% increase in carbon emissions due to tropical forest clearing. Recently, a high-resolution map quantifying gains and losses in global tree cover was produced using vegetation tree cover percentage determined from Landsat imagery [67]. Global Land Cover (GLC)'s land monitoring services provide global land cover and vegetation physiological products (LAI, FCover, and FAPAR) derived from Project for On-Board Autonomy-Vegetation (PROBA-V) (2014 to present at 100 m and 300-m resolutions) and Satellite Pour l'Observation de la Terre (SPOT) vegetation (1991 to preset at a 1-km resolution) image time series [78]. The GLC is an initiative developed under the ESA's Copernicus program (https://land.copernicus.eu/global/), and the products have recently been integrated with Sentinel 1 and 2 time series for continuity [69,70,78].

3.2.1. Leaf Area Structure

Density, structure and distribution of leaves in a canopy are vital components for understanding, modelling and upscaling of ecological structure and carbon dynamics of the forest ecosystems [94,95]. LAI refers to "the total one-sided area of leaf tissue per unit ground surface area" [96]. The leaf area structure of canopies influences the NPP and evapotranspiration, and, hence, it is imperative for carbon biomass and flux monitoring models that are sensitive to canopy depth [97,98]. Conventional optical (passive) remote sensing provides LAI and amount of leafy biomass as a proxy parameter to canopy leaf function and leaf quality for ecological processes modelling [99]. It is a physiological index derived from spectral properties related to photosynthesis [9]. Optical measurements of LAI are carried through various sources, ranging from in situ hemispherical photographs to space-based multispectral radiometers. However, LAI measurements suffer from potential uncertainties associated with sensor saturation with high LAI levels (greater than an order of three to five) on dense canopies due to reflectance, transmittance and absorption of the signal along the full canopy vertical column [100,101].

In addition to LAI, Leaf Area Density (LAD), volumetric distribution of leaf area and three-dimensional canopy leaf structure, has emerged as a critical parameter, determined through remote sensing data to understand canopy profile (horizontal and vertical structure of canopy leaves) and canopy light environment for forest biomass estimation and carbon flux monitoring [102]. It is important to note that passive remote-sensing-based LAI measurements do not effectively incorporate vertically resolved leaf area profiles but rather suffer saturation errors. Nonetheless, active (Radar and LiDAR-based remote sensing) as well as the integration of active and passive methods perform better by incorporating the 3-D canopy structure and do not saturate over dense canopies [100,103]. In tropical forests, active remote-sensing-based estimation of LAI and/or LAD are significantly important due to

saturation and the cloud cover problem in passive remote sensing applications. Almeida et al. [104] determined the optimal values of laser point cloud pulse density (>15 pulses m^{-2}) and grain size (<10 m) for a stable estimation of LAD profile using Airborne Laser Scanning (ALS) data in a dense tropical rainforest at the Ducke Forest Reserve, Brazil. Leaf area profiles derived from remote-sensing-based LiDAR mapping has been used to simulate tree size, distribution and canopy structure in the Amazon forests [103]. Shao et al. [9] assessed the canopy dynamics of leaf area structure in the Amazonian forests and found that bias-corrected LAI and LAD derived from LiDAR data can detect canopy structure at the ecologically significant scale of 0.25 ha. They concluded that it is difficult to estimate LAI and LAD from the air or space-borne LiDAR scanning systems, due to landscape heterogeneity and its sensitivity to sensor type, flight dimensions and time of data acquisition [9].

At the pan-tropical scale, vertical foliage profiles derived from the Geoscience Laser Altimeter System (GLAS)/Ice, Cloud, and Land Elevation Satellite (ICESat) LiDAR data have been combined with MODIS and Landsat datasets to produce high-resolution carbon density maps of tropical forests [105]. Zhu et al. [106] produced the third generation of 15-day global LAI, FAPAR and Normalized difference vegetation index (NDVI) products, by applying Neural Network algorithms on GIMMS and MODIS LAI at a 0.083-degree spatial resolution since 1981 to December 2015. Tang et al. [107] produced global LAI and VFP (Vertical Foliage Profile) from GLAS/ICESat LiDAR data integrated with pre-processed MODIS LAI and another GLAS-based estimate using the Geometric Optical-Radiative Transfer (GORT) model. Recently, reliable LAI and LAI profiles measurements have been produced from space-borne LiDAR data by the Global Ecosystem Dynamics Investigation (GEDI) at a higher resolution of 25 m [108].

3.2.2. Canopy Height

Canopy height or tree height is a critical parameter for quantification and modelling AGB as the biomass increases with increasing size of the tree [109,110]. Continuous measurement of the two world's tallest tree species *Sequoia sempervirens* and *Eucalyptus regnans* showed that the AGB significantly correlates with age and height of the tree [111]. However, the dense structure of tropical forests impedes conventional ground-based measurements (telescoping height measuring pole, tangent methods, laser range finder, etc.) of canopy structure and the accuracy of the measurements is significantly influenced by the method being used and/or expertise of the surveyors [112]. The rapid development of remote-sensing-based technologies can overcome these difficulties by providing accurate and repeatable estimates of the canopy models in dense tropical forests. For instance, ALS can provide a three-dimensional model of the multi-layered forest structure as the laser can penetrate the upper canopy layers. A study in the tropical forest of Africa achieved an accuracy of 0.64 while estimating AGB from the canopy height metrics derived from airborne LiDAR [113]. However, the mapping accuracy was improved to 0.70 when the LiDAR-derived canopy height metrics were combined with hyperspectral data to estimate the AGB. The scarcity of the LiDAR data due to the cost and logistic arrangement is one of the major limitations for contagious mapping of AGB estimates. However, efforts have been made to integrate LiDAR derived canopy height with high-resolution optical images ('Planet Dove'satellite imagery at a 4 m spatial resolution) for country-level estimates of AGB in Peru. The study achieved the correlation of 0.70 with an RMSE (root-mean-square error) of 25.38 MgC per ha [114]. Similarly, another study derived AGB estimates by calculating mean tree canopy height using airborne LiDAR observation at a 1 ha spatial resolution and then extrapolated the results by integrating it with spatially contiguous environmental variables [34]. The accuracy of AGB estimates from ALS data is influenced by the spatial resolution (inversely proportional to the square root of plot area) and 10% error could be expected while producing LiDAR-based AGB maps at a 1 ha spatial resolution [115]. Furthermore, airborne LiDAR data have been demonstrated to increase the accuracy by ~40% of AGB estimates from freely available medium-resolution remote sensing images [116]. Spaceborne LiDAR altimetry observation from GLAS onboard ICESat-1 [32,105], Advanced Topographic Altimeter System (ATLAS) onboard ICESat-2 [117–119] and the GEDI onboard International Space Station (ISS) [108] are extensively being used for developing forest canopy and height parameters which are essential

for AGB estimation models [23]. Recently, a forest canopy height map of 2019 at a 30 m spatial resolution is released by the UMD GLAD [120,121]. The global forest canopy height map is derived from combined analysis of LiDAR observation acquired by the GEDI and time series of the Landsat. However, this forest canopy height map can underestimate forest canopy heights above 30 m and direct use of this product may require further investigation.

3.2.3. Forest Age Class

Apart from vegetation structural classes (e.g., Forest, Shrub, and Grass), successional age groups of forests are important for the estimation of changes in NPP, NEP, biomass as well as carbon flux, especially in recovering tropical secondary forests [61]. These maps could be prepared through sequential analysis of high-resolution aerial photographs or satellite images [12,122,123] and/or spectral profiles of different age groups of the forests [124], and spectral recovery indicators from time series of medium-resolution multispectral images. Earlier, multispectral analysis of multitemporal Landsat images is used to estimate the age of the recovering topical forests in Amazon [125]. Another Landsat-based study estimated the age of the regenerating tropical forest in the Tapajos National Forest of Brazil by performing multitemporal analysis [126]. Both the studies [125,126] documented the utility of NDVI in determining the age classes of secondary forests. A recent study documented a significant difference in fluorescence emissions (which is a proxy variable for plant biomass or carbon flux measurement) among different age groups of Hong Kong's recovering tropical forests [127]. They observed higher productivity up to the age of 61 years old and then a decline in productivity in the old-growth forests. This accords with fairly recent pronouncements by scientists that older forests are not as efficient as younger rapidly growing forests as carbon sinks. Espírito-Santo et al. [128] presented a multitemporal semi-automatic classification approach to map successional stages of the recovering tropical forest in Brazilian Amazonia using Landsat images. Another study in the Brazilian Amazon presented an integrated analysis of multispectral Landsat and ALOS PALSAR images to determine the age of secondary forests [129]. Recently, annual forest age maps of a 33-year (1985–2018) secondary forest succession in Brazil have been produced by using the time series of LCLU maps (MapBiomas Project Collection 4.1) derived from Landsat satellite images [71]. Apart from satellite remote sensing time-series studies, multitemporal photogrammetric analysis of aerial photographs has shown strong potential to determine the structural changes and age of tropical forests [130].

Recent studies are indicating changes in vegetation productivity along successional gradients from new young forest to old-growth primary forests. For example, Zhou et al. [131] quantified a relationship between forest age and carbon sink and found that carbon sequestration capacity gradually increases and peaks after 22 years, then start declining. Another study found a temporal pattern of the rapid increase in NPP in USA forests at the young ages, peak growth in the middle ages, and a slow decline in the mature ages [132]. Ryan et al. [133] linked the declining patterns of forest growth with a decline in photosynthesis and dry matter production once a canopy achieves a maximum leaf area. Besides, it has been documented that the forest-age and height are both controlling factors of photosynthesis in Amazonian forests [134]. They also found that the younger and shorter forests are three times more sensitive than the older forests to precipitation variability, due to lesser biomass and lack of deeper roots to access deeper moisture soil. Thus, successional age classification map provided by remote sensing can improve the ability of NPP and NEP simulation models, by simulating carbon cycles processes along successional age gradients [135]. Consequently, the availability of long-term records of low- and high-resolution satellite records of the past five decades, together with a cloud computing platform, would enable the production of high-resolution forest age maps that would play a significant role in future studies of the remote-sensing-based estimate of carbon stock assessment in the tropical secondary forests.

3.2.4. Phenology Cycle

Phenology of evergreen tropical forests is controlled by the emergence of new leaves, their maturity and shedding of old leaves [136]. However, the magnitude and variations in photosynthesis seasonality are less prominent compared to phenological cycles in other ecosystems [51]. The seasonality of the tropical forest significantly influences the carbon stock and GPP [137]. In the old-growth Amazonia tropical forests, Xu et al. [138] identified nine distinct phenological zones indicating GPP seasonal cycles, by combining monthly MODIS LAI/EVI, AMSR-E vegetation optical depth (VOP), GRACE terrestrial water storage (TWS), Clouds and the Earth's Radiant Energy System (CERES) Photosynthetically active radiation (PAR), and Tropical Rainfall Measurement Mission (TRMM) precipitation measurements. Thus, knowing phenological characteristics, the timing of green-up and senescing, and changes in leaf area and density over the growing season are critical while assimilating and interpolating carbon stock measurements in tropical forests [47,139]. Many satellite-based phenology products, such as from AVHHR, MODIS, SPOT vegetation, Medium-Resolution Imaging Spectrometer (MERIS), with varying spatial resolutions (8 to 100 m), have been developed by the scientists which are now an imperative part of the carbon cycle and stock measurements in the tropics and elsewhere in the world [37,51,87]. Recently, continental-scale Land Surface Phenology (LSP) has been produced by combining time series of images Landsat 8 (30 m) and Sentinel-2 (10 m), which can capture finer details of variation in phenology and AGB across various biomes [140].

4. Changes in Tropical Forest Cover

Estimating carbon losses and gains from deforestation and degradation, and regenerating secondary forests in the tropics, plays a critical role in contemporary carbon budget monitoring [141]. However, it is highly uncertain to obtain spatially explicit and consistent information on carbon exchange, due to dynamic forest cover and land-use changes in tropical ecosystems. Nonetheless, various studies have attempted to quantify tropical forest cover changes and associated carbon fluxes using remote sensing observations at various spatial and temporal scales. For instance, Figure 4 represents a Landsat-based assessment of status and distribution of tropical woodlands and forests indicates the distribution of intact (a minimum mosaic of forest and naturally treeless ecosystems of 500 km^2 with no sign of human activity), fragmented/managed, deforested and degraded tropical woodlands and forests [142]. The study reported that the loss of intact tropical landscape is increased by three times during 2011–2013 than during 2001–2003 [83,142,143]. In 2002, DeFries et al. [93] quantified tropical forest cover changes from 1982 to 2000 using coarse resolution (8km) daily satellite images of NOAA's AVHRR. They estimated yearly sub-pixel level Percent Tree Cover (PTC) from the satellite time series, and used median values of the PTC to derive forest cover changes in three intervals, 1982–87, 1988–92 and 1993–99. Later, they integrated the PTC with "bookkeeping terrestrial carbon mode [144]" to estimate pixel-level carbon flux dynamics in the tropical forests. They found the net annual rate of tropical deforestation has increased by ~10% (accelerated deforestation) from 5.04 million ha yr^{-1} in the 1980s to 5.563 million ha yr^{-1} in 1990s, which resulted in a net annual carbon flux loss of 0.6 Pg (600 Mt) and 0.9 Pg (900 Mt). Notably, these estimates of the rate of deforestation are lesser by 35.3% and 62.6% from the estimates of 13.463 million ha yr^{-1} and 8.6 million ha yr^{-1} by the FRA reports for the 1980s and 1990s.

Similarly, a Landsat-based assessment, at the spatial resolution of 30 m, of tropical forest cover changes, indicated tropical deforestation at an annual rate of 0.49% with a gross loss of 8.0 million ha yr^{-1} from 1990 to 2000 and 7.6 million ha yr^{-1} from 2001 to 2010 [145]. This work was carried through a systematic sampling approach and statistical extrapolation of the results. Notably, 54% of the forest loss during the 2000s occurred in humid tropics which occupies 64% of the tropical forests [145]. Besides, overlay analysis of these change maps with pan-tropical biomass maps (Figure 5) resulted in a net loss of 883.5 MtC [0.88 PgC] per year from 1990 to 2010 [145]. On the other hand, the emergence of the secondary tropical forests on abandoned agricultural land has removed 106 MtC (0.11 PgC) annually [145].
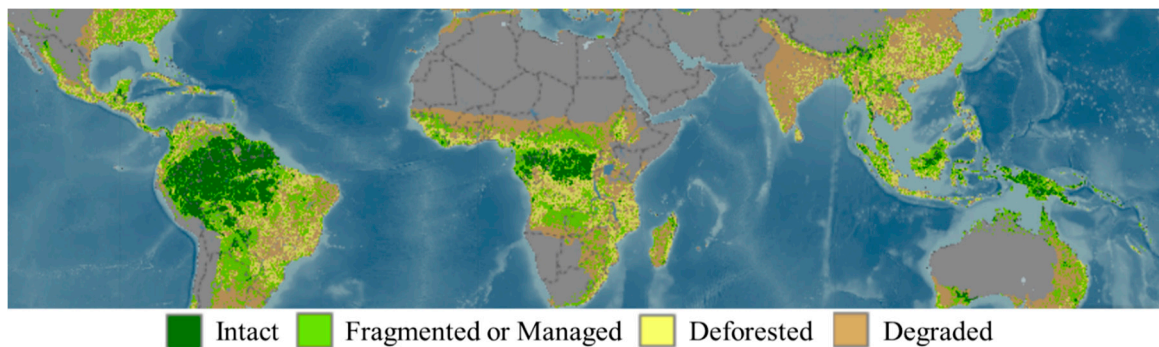
Figure 4. Distribution of intact, fragmented/managed, deforested and degraded tropical woodlands and forests in 2011 [142].

Furthermore, based on 5444 Landsat images acquired during 1990, 2000, 2005, and 2010, Kim et al. [15] observed a 62% acceleration in deforestation rates in the humid tropic from the 1990s to 2000s. Conversely, there is a more general agreement emphasizing the decreasing trend in deforestation in the humid tropics during the 1990s to 2010s [6,145]. Achard et al. (2014) also used the Landsat images for 1990, 2000 and 2010 to estimate tropical forest cover change. They used an image segmentation approach with an MMU of 5 ha and reported a reduction in deforestation in tropical forests from 8.0 million ha in the 1990s to 7.6 million ha in the 2000s. According to FAO's FRA 2020 [146], the rate of net global forest loss has reduced gradually from 7.8 million ha during the 1990s to 4.7 million during 2010s. The largest proportion (90%) of global deforestation was in tropical countries. Interestingly, the rate of deforestation has gradually decreased from 13.8 million ha in the 1990s to 13.2 million ha in the 2000s. During the last decade (2010–2020), a significant reduction is reported, and the average rate of deforestation drops to 10.3 million ha during 2010–2015 and 9.3 million ha during 2015-2020. This reduction of net forest loss results from a decrease in deforestation as well as an increase in recovering secondary forests, expansion of existing forest and plantations [6]. In another study, a global forest cover change assessment from 2000 to 2012 was performed, using Google Earth Engine's cloud computing platform and Landsat satellite images [67]. They reported ~7.1 million ha deforestation every year in the tropical forests. These forest cover change, losses and gain maps are now updated yearly by the GLAD and hosted on the online portal of GFW. Most of these studies used satellite images for forest cover assessment, and the primary differences in estimates lie in the assessment approach, viz. inherent classification errors [147], sampling-based approach [145], sample size and distribution of samples, spatially contiguous or wall-to-wall assessment [15,63,67], systematic or stratified sampling methods, MMU as well as definitions of 'forest', 'deforestation' and 'degradation'. Differences in remote sensing methodologies, assessment period and forest definition impede comparative assessment of change statistics among different studies [148].

For example, Achard et al. [145] and Kim et al. [15] defined the forest as a patch of land with greater than one ha in area and comprising pixels with greater than 30% tree cover, while Hansen et al. [67] and FAO's FRA [149] considered 25% and 10% of tree cover in a greater than one ha patch to classify it as forest. It is important to note that the automatic mapping and forest definition can classify young (re-growing) vegetation as well as oil palm and rubber plantations as forests. For example, in the study by Kim et al. [15], overestimation of the forest cover extent for the year 2000 leads to an underestimation of deforestation during the 1990s and an overestimation of forest cover loss during 2000s. Moreover, the unavailability of high temporal frequency Landsat images during the 1990s coerces to use longer time steps as compared to shorter time steps in the 2000s. The use of different time steps can lead to serious errors when estimating the rate of deforestation in different decades. For instance, Kim et al. [15] used two different time steps for the 1990s (1 × 10 year) and 2000s (2 × 5 yeas) which can lead to picking up more changes during 2000s in dynamic tropical landscapes such as shifting cultivation areas and tree plantations. However, FAO's FRA 2020 also used different time steps to estimate forest

loss in the 1990s (1 × 10 year), 2000s (1 × 10 year), and 2010s (2 × 5 year) but reported a continuous reduction in deforestation [6]. Subsequent regrowth of forests is difficult to identify, especially using medium resolution (Landsat) images with a shorter assessment period (less than a decade), and it requires significant input from ground field surveys to evaluate whether the changes are temporary or permanent [150]. Similarly, as discussed in Section 3.1, a lack of cloud-free images during the 1980s and 1990s contributes to uncertainties in forest cover extents, which might contribute to the underestimation of deforestation rates during the period, especially when using Landsat images in humid tropics. Furthermore, it is difficult to avoid the analyst bias even during the interpretation of land cover with the best available reference data. This bias can be minimized by involving several interpreters and automatic methods [151]. In another study, Bos et al. [152] found significant user and producer inaccuracy in tropical forest region of Global Forest Change (GFC) datasets. They showed that the accuracy of forest cover loss from such products could be increased by incorporating high-resolution imagery. Moreover, the availability of historical data and reliable baseline data is necessary for the accurate estimation [153], which is missing in many under-developed countries.

However, the prevailing trend of data availability and algorithm, open data science, on cloud computing platforms such as GEE can open new arenas to enhance the mapping accuracies by incorporating knowledge of local- or national-level researchers and synchronizing results from different studies. Moreover, the global forest change datasets, such datasets hosted on the GFW, can provide reasonable results for national-level forest measuring, reporting and verification (MRV) requirements after adjusting the percentage of tree cover according to localized standards. Nevertheless, independent high precision ground reference information would be required to derived annual forest cover change maps across regions with different levels of degradation, such as in pan-tropical studies [154].

5. Tropical Deforestation and Carbon Emissions

Tropical forests are great carbon sinks. Around 10% of the global carbon emissions are added through the degradation and deforestation of tropical forests [114] and a net loss of 1.0 PgC stock per year from 2000 to 2010 [105]. It is important to understand the changes in the AGB of tropical forests for their significant role in climate change mitigation policies to increase net carbon sink under REDD+ initiatives. The Intergovernmental Panel on Climate Change (IPCC) has devised a default rate of change in AGB in tropics, which is based on the outcome from several studies. This net rate of change in AGB does not account for the age of forests considered given that, in tropical areas, the forest is re-growing and much of the tropical forests can be classified as secondary forest. The authors of [155] have updated the estimates of the rate of change in AGB in tropical countries using field inventory data from 176 plots in secondary and 536 plots in primary tropical forests. However, these rates are spatially constrained and do not imply across the tropics. Therefore, remote-sensing-based upscaled and spatially continuous estimates of carbon density changes in tropical forests are required for the monitoring and understanding of gains and losses in the AGB. Conventional remote sensing approaches rely on forest cover change integrated with forest density. For example, Pan et al. [4] used forestry inventory data and country-level remote-sensing-based ecosystem carbon studies, for 1999 to 2007, to estimate annual rates of net carbon emission (2.9 PgC) and sink (2.8 PgC) from tropical forests. A similar rate of emission, 1.0Pg carbon stock per year from 2000 to 2010, is reported by Baccini et al. [105] due to deforestation and degradation in tropical areas. In another study, the gross rate of carbon emission from tropical areas is estimated to be 0.81 PgC during 2000 to 2005, using a combination of field plot data and multi-sensor remote sensing images of MODIS, Landsat ETM+ and LiDAR [92]. In recent years, a combination of optical and airborne LiDAR datasets has emerged as a common practice among scientists to estimate aboveground carbon stocks in tropical forests. Many other significant studies applied remote sensing techniques to estimate pan-tropical carbon losses and gains [145,156–158]. Recently, a pan-tropical quantification of the net change in carbon density of tropical woody vegetation has been made [159]. Primarily, this study is based on field inventory data, LiDAR measurements and pan-tropical MODIS images spanning over 12 years (from

2003 to 2014). It is revealed that the tropical forests are a source of CO_2 with an annual release rate of 0.425 PgC. Moreover, 30 m Landsat-based maps of tree cover percentage [67] were used to distinguish carbon losses from forest cover loss and degradation/deforestation. Overall, carbon is sequestrated at an annual rate of 0.436 Pg, while deforestation and degradation of tropical forests have released 0.861 Pg of carbon per year. In contrast to this, a few studies found that the tropical forest is a net sink of carbon, absorbing carbon at a net annual rate of 1.4 PgC [7]. A recent study by Hubau et al. (2020) [160] found asynchronous patterns of carbon sinks in the tropics. The African tropical forest and Amazonian forest both showed an unparallel increase in carbon loses. Carbon sinks in intact African tropical forests have been stable for the past three decades, until 2015, as compared to a continuous decline in Amazonian forests' carbon sink. This difference is largely due to the increasing tree mortality in Amazon forests. Both continents showed an increase in tree growth. However, since 2010, an increase in carbon losses in African forests has been observed, indicating saturation of the carbon sink potential of intact old-growth tropical forests in Africa. An overall global carbon sink is increasing with a greater increase in the Northern Hemisphere [160]. Generally, limited availability of field data, an approach adapted for analysis, the difference in reference levels, a period of assessment, a definition for forest, analysis scale and the exclusion of post-deforestation regrowing tropical forests can induce serious uncertainties in carbon sinks and emission [4]. The segregation of causes of forest degradation or deforestation is important to consider, while estimating net loss in carbon sinks because of, for example, disturbances due to natural disasters (frost, typhoon, drought) has the potential to recover over time as compared to transitions of forest cover to other land use types, although both disturbances can be reverted but the time of recovery and sink potential can vary significantly [161].

6. Pan-Tropical AGB Mapping

The quantification and mapping of changes in spatial distribution and patterns of AGB, in tropics, is a key parameter to estimate carbon uptake and emissions induced by the LCLU change and its impacts on global climate changes [105]. Apart from site-specific or localized AGB estimates using a variety of modelling approaches, efforts have been made to develop pan-tropical or global AGB estimates (Tables 2 and 3) by integrating ground inventories and remote-sensing-based forest products (described in sections above). The first pan-tropical map of live biomass was produced at a 1-km spatial resolution in 2011, by combining extensive filed inventory data from 4079 plots and a variety of remote sensing methods acquired by optical, microwave and LiDAR sensors [156]. The total woody biomass of the tropical vegetation was estimated to store 247 PgC, with 78% contribution of carbon stock from AGB, and the remaining 22% of the carbon stock was attributed to below the canopy biomass of roots. Later, in 2012, another pan-tropical AGB map was produced at a 500 m resolution using a multiscale multi-sensor mapping and calibration approach by combining field inventories, GLAS LiDAR data at 70 m resolution and MODIS multispectral surface reflectance images at a 500 m resolution [105]. Moreover, a carbon density map ($MgC\ ha^{-1}$) was produced for the improved estimation of carbon emissions from tropical deforestation and degradation [105]. The study showed that 228.7 PgC is stored in the tropical woody vegetation, which was 21% higher than the FAO's estimates in the FRA report of 2010, with a net carbon emission of 1.0 $PgC\ yr^{-1}$ from tropical deforestation during 2000–2010 [105]. Measuring and mapping carbon stock and fluxes in tropical areas is challenging, due to uncertainties in canopy structure and height parameters and the advection effect induced by small topographic variations. Therefore, it is difficult to extrapolate plot-level AGB estimations to pan-tropical areas. Considering the challenges in the pan-tropical biomass estimation and limitation of the two previous studies [105,156,162], an updated pan-tropical AGB map (Figure 5) was produced by integrating the existing two pan-tropical biomass maps, along with the harmonization and upscaling of field inventories, and additional reference, consolidation, local AGB estimates, and other covariate datasets [163]. The updated map, estimated AGB carbon stock of 375 Pg dry mass in the tropics, which is 9% and 18% lower than the previous dry mass estimates of 413 Pg [156] and 457 Pg [105]. Santoro and Cartus [164] has produced recent estimates of the global forest AGB at a 100 m spatial

resolution as part of ESA's CCI. The algorithm is primarily based on the two SAR products acquired in 2017—a global mosaic from PLARSAR-2 (onboard ALOS-2) operated by JAXA and another set of SAR data acquired by Sentinel-1 operated by ESA—as well as the LiDAR data from the ICESat. Recently, a new approach is developed to harmonized measures of aboveground vegetation biomass and belowground biomass across the globe at a spatial resolution of 300 m for the year 2010 [165].

Mitchard et al. [166] assessed pan-tropical biomass maps produced at 500 and 1000 m spatial resolutions, and they found substantial uncertainties when compared with the FRA country-level data and with the 100 m biomass map. They found that both pan-tropical maps have higher biomass estimation when compared with a high-resolution map. Large uncertainties are related to the spatial distribution of biomass and spatial pattern of forest landcover change. Similarly, uncertainties and inaccuracies in measuring AGB and carbon emission by different countries were reported by "forest reference emission levels and forest reference levels" FREL/FRL 2020 [167]. Between 2014 and 2016, five out of seven countries who submitted national-level carbon stock have aggregative uncertainties. Primarily, the ambiguities arose due to the exclusion of post deforestation carbon content in the estimation reports. Recent studies submitted to FREL/FRL made sure that carbon content must be included in the post deforested land in their carbon emission estimations [167]. Uncertainty analysis is important in assessing the estimations of carbon emissions by deforestations studies. Three steps are important in uncertainty analysis, including the identification of the estimation uncertainty source and quantifying the sources of uncertainty and aggregation of all uncertainty to conclude the final uncertainty value. IPCC guidelines Tier 1 document the uncertainty analysis and different organizations and countries apply this methodology. The Monte Carlo simulation approach is recommended for carbon estimation studies [168].

IPCC Tier 1 maps are still the primary source of AGB estimation maps which are based on "stratify and multiply" mapping technique and represent the year 2000 and provide a detailed wall-to-wall product but advancement in recent technologies such as high-resolution maps and detailed field surveys showed that this method of estimation of AGB increases the error and uncertainties. Spawn et al. [165] developed a methodology using 300 m spatial resolution datasets for the AGB map of 2010 but were advised not to use it in comparison with the IPCC Tier 1 AGB map because of a significant difference in methodologies and that it should only be used for global studies.

Table 2. Remote-sensing-based datasets of Pan-tropical biomass mapping (arranged by the year of publication).

Study	Year	Data Used	Attribute
Spawn et al., 2020 [165]	2010	Harmonization of existing biomass products	Above and below-ground biomass carbon density at 300 m
Santoro and Cartus, 2019 [164]	2017	PALSAR-2 Sentinel-1	Global AGB biomass of 2017 at 100 m resolution
Avitabile et al., 2016 [163]	2010	Updated from Saatchi [156] and Baccini [105]	Improved pan-tropical biomass at 1 km
Santoro et al., 2015 [169]	2010	Envisat ASAR	Topical forest AGB at 1.1 km
Baccini et al., 2011 [105]	2010	GLAS LiDAR, MODIS, SRTM	Pan-tropical AGB at 0.5 km, and change assessment 2000-2010
Saatchi et al., 2010 [156]	2001	GLAS LiDAR, MODIS, QSCAT, SRTM	Pan-tropical total biomass carbon at 1 km

Table 3. Remote-sensing-based assessment changes in pan-tropical biomass (TgC year^{-1}) (arranged by the year of publication).

Study	Period	Data Used	Gross Loss	Gross Gain	Net Change	Remarks
Pan et al., 2011 [4]	1990–1999 2000–2007 1990–2007	Multiple remote sensing products	3030 2820 2940	2900 2740 2830	130 80 90	Gross deforestation emissions. Include soil respirations or carbon
Baccini et al., 2012 [105]	2000–2010	MODIS, GLAS LiDAR, SRTM DEM	810	480	330	–
Harris et al., 2012 [92]	2000–2005	MODIS, Landsat, LiDAR	810	–	–	Forest cover change does not include losses due to degradation and deforestation
Achard et al., 2014 [145]	1990–1999 2000–2010	Landsat	887 880	115 97	772 783	Gain is calculated from regenerated forest
Tyukavina et al., 2015 [157]	2002–2012	Landsat, LiDAR	1022	–	–	Forest cover change does not include losses due to degradation and deforestation
Baccini et al., 2017 [159]	2003–2014	MODIS, LiDAR, Landsat	861.7	436.5	425.2	–
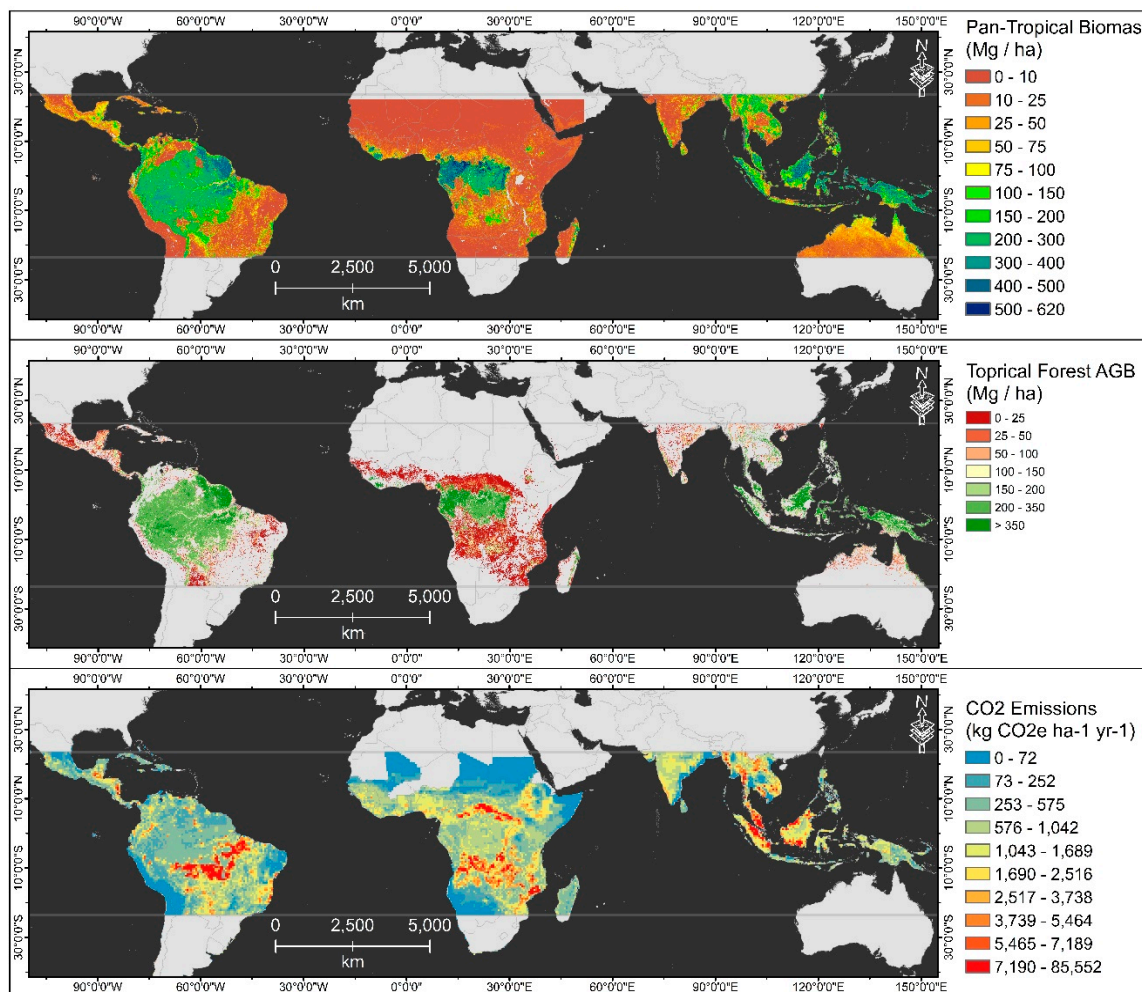
Figure 5. Spatial distribution of total pan-tropical biomass [163], tropical forest AGB for 2010 [169] (Another dataset for 2017 is recently released by the ESA [164]), and net emissions of CO_2 from tropical areas for 2000–2015 [170].

6.1. Country-wide High-Resolution Tropical Biomass Mapping

Apart from low-resolution pan-tropical estimates of tropical biomass, numerous studies have been conducted to estimate biomass on national or limited geographic scales by using the high-resolution passive or active remote sensing data. Free availability of medium-to-high-resolution images (such as Landsat and Sentinel-2 imagery at 30 m and 10 m spatial resolutions), rapid progress in cost-effective airborne systems and high-performance computing systems have enabled the possibility of mapping the tropical carbon stock monitoring at a higher resolution. Recently, Forkuor et al. [171] mapped AGB in West African tropical dry forests by applying a Random Forest machine learning algorithm on integrated SAR images of Sentinel-1 and multispectral images of Sentinel-2. They found that multispectral images produced better results than the SAR images. However, the best results were achieved by combining the two. A random forest regression model was effectively used to estimate the high-resolution AGB map of Peru by combing the textural and reflectance features derived from high-resolution 'Planet Dove' satellite images (4 m spatial resolution), and canopy height information from LiDAR datasets [114]. Earlier, Asner [33] presented an integrated approach of combining airborne LiDAR data with the Landsat-based forest attributes (such as canopy cover, deforestation and degradation), which were obtained through the Carnegie Landsat Analysis System (CLAS) developed for the Brazilian tropical forest monitoring and assessment using a variety of satellite imagery [35]. This analysis is based on the allometric equations derived from extensive in situ measurements of tree diameters, height and wood density [38,172]. Gascón et al. [173] explored the potential of Rapid Eye imager (5 m spatial resolution) for national-level carbon stock assessment of Tanzania by first segmenting the image into image object of 1 ha, and then applying a random forest regression between the image objects feature (textural, spectral indices and reflectance) and field-based estimates of AGB. In another study, an object-based method was developed by integrating very-high-resolution Quickbird-2 imagery with LiDAR data to estimate AGB in the tropical forest of Cambodia [174]. In Central Africa, very-high-resolution images acquired by the GeoEye-1 and Quickbird-2 satellites were used to produce the high-resolution biomass map (100 m), by developing the piecewise regression model from the 26 inventory plots and canopy texture metrics—Fourier Textural Ordination—derived from the optical satellite images [175]. Singh et al. [176] developed a framework of modelling the AGB of the tropical forest in Southeast Asia, by applying Random Forest and a Support Vector Machine (SVM) on textural indices—Grey Level Co-Occurrence Matrix, Fourier-Based Textural Ordination (FOTO) and Gabor Wavelet-Based Texture Measures—derived from Google Earth images at a 50 cm resolution, and very-high-resolution multispectral aerial images at an 8 cm resolution. Similarly, a combination of FOTO and Lacunarity textural feature and bioclimatic proxy variables was used to develop a generalized prediction model of AGB. This study was based on 279 samples of 1 ha plots distributed in three continents (India, Africa and French Guiana). The model was tested using the textural features derived from high-resolution (0.7 to 1 m) Pleiades images and another set of validation data comprising 49 plots of 1 ha in Eastern Cameroon [177]. Texture-based modelling of the spatial gradient in tropical AGB has gained popularity among scientists over the past 10 years, and these studies have opened new possibilities of using high-resolution low-cost images for estimating AGB biomass in tropical forests at the landscape level. However, the scope of biomass estimation using the very-high-resolution commercial satellite imagery is limited to smaller geographic areas due to its availability and cost.

6.2. Concepts, Approaches, Coping Capacities and Limitations

Several international organizations are working together under the umbrella of UN programs, as well as independently, to improve mapping, monitoring, validation and reporting of net forest and carbon loss across the globe. The Global Forest Observations Initiative (GFOI) was established by Group on Earth Observations (GEOs) in 2011, provides satellite-based forest measurements as well as field-based methodologies for the production of globally consistent reports and reliable findings

on forest cover change, forest use and greenhouse gas (GHG) emission and removals accounting for REDD+ activities [178].

According to the IPCC's guidelines, forest carbon stock assessment can be categorized into three Tiers ranging from the simple global/ecological zone level emission factor (Tier 1) to country-specific forest inventories (Tier 2) and high precision plot level carbon dynamics models [178,179]. The Global Observation of Forest Cover and Land Dynamics (GOFC-GOLD) which is an ad-hoc REDD working group of international experts, facilitates scientific communities, national space agencies and remote sensing analysts to maintain standards while using Earth Observation (EO) datasets [180]. REDD+ has had significant progress during the last decade. REDD+ helps developing countries to become part of their program to reduce carbon emission and enhance forest sinks. The UNFCC report published regularly to update nations about the latest development in the understanding of MRV for REDD+ activities [167].

The United Nations Strategic Plan for Forests (UNSPF) 2030, UN forum on the forest, set six global objectives for forests to be achieved by 2030, including intent to reverse forest loss, improvements in forest-dependent people livelihood by enhancing forest-based benefits, the sustainability of forest management to increase the area of protected forest, mobilization of financial resources for forest management, governing framework for forest management and enhance cooperation, coordination and synergies [181].

The FRAs coordinated by FAO publishes recent trends in forest studies and updates of technical terms after every five years to maintain consistency. The FRA 2020 [6] adapted internal forest policy such as Agenda 2030 for Sustainable Development, the UNSPF-2030 and the Paris agreement. Their working paper improves the understanding, definitions and terminologies for forest resources; assessments and countries are advised to strictly follow its guidelines.

The recent report by FAO in 2019 [167] provided a technical assessment of carbon stock of thirty-nine countries. Out of these, eight countries reported more than 8 billion tons of carbon emissions reduction mostly by Brazil. Reports from six countries, which submitted the Forest Reference Emission Levels (FREL) and REDD+ reports, indicate uncertainties in the estimation of forest emission. Based on these reports, a major source of the uncertainties was the assumption of total carbon loss from the AGB, below-ground biomass (BGB), litter (l) and deadwood (DW) carbon pools due to deforestation. They did not consider the removal of carbon from subsequent vegetation growth and post-deforestation land use. Only Cambodia, Chile, Ghana, Indonesia, Lao People's Democratic Republic, and Vietnam submitted the reports with the use of remote sensing and field inventories [167].

Despite positive advancement in global effort in providing guidelines and giving incentive to countries to implement reforestation strategies, recent studies suggest that many uncertainties occur in the estimation of AGB and the detection of the total forest land. More emphasis should be given to capacity building programs, such as FAO and REDD+, to enhance capacities of developing countries to maintain and streamline national forest monitoring efforts which require continuous positive corrections and adjustment in their mapping and reporting mechanisms [182]. Figure 6 indicates the distribution of capacities of the tropical countries in using remote sensing to developed forest inventories and change assessment mapping according to REDD requirements and guidelines. Most of the carbon pool reporting countries are still at the Tier 1 level of IPCC guidelines. This indicates major improvement is required in mapping capacities for the country-level reporting to achieve the Tier 3 level. Langner et al. (2014) [183] reported that the IPCC values of emission factor, especially using Tier 1, do not give accurate estimates, especially in tropical forests that mostly consist of a mixed and multilayer dense canopy forests. Thus, the IPCC standards do not represent ground reality. That is because of numerous uncertainties present in the field data which cannot be solved through conventional methods and statistical approach for which IPCC does not provide a specific guideline. It is suggested to use Saatchi [156] and Baccini [184] datasets for the better alternative to IPCC Tier 1 values [183]. Furthermore, the IPPC 2006 defined two broad categories, less than 20 years forest or greater than a 20-year forest, to calculate the change in biomass over time. However, as part of the

"2019 Refinement to the 2006 IPCC Guidelines for National Greenhouse Gas Inventories", Requena Suarez et al. [155] further divided the forest into three categories, including young secondary forest (≤20-year-old), older secondary forest (>20 to 100-year-old) and old-growth forest. The gain in biomass decreases with the maturity of the forests from the younger forests (≤20 years) to mature and old-growth forests [155]. Recently, De Sy et al. (2019) [185] showed that agriculture land dominated the land use after the deforestation occurred between 1990 and 2000 but a different type of post-deforestation agriculture land-use practices are followed in different countries. Carbon stock of ecozone was higher than those of deforested areas. They refined emission factors by integrating the post-deforestation LCLU type with the pan-tropical biomass map at a 30 m spatial resolution. Large uncertainties were found in pan-tropical AGB maps with little or no field data but utilizing the refined maps can help in estimation of carbon stock assessments studies [185].
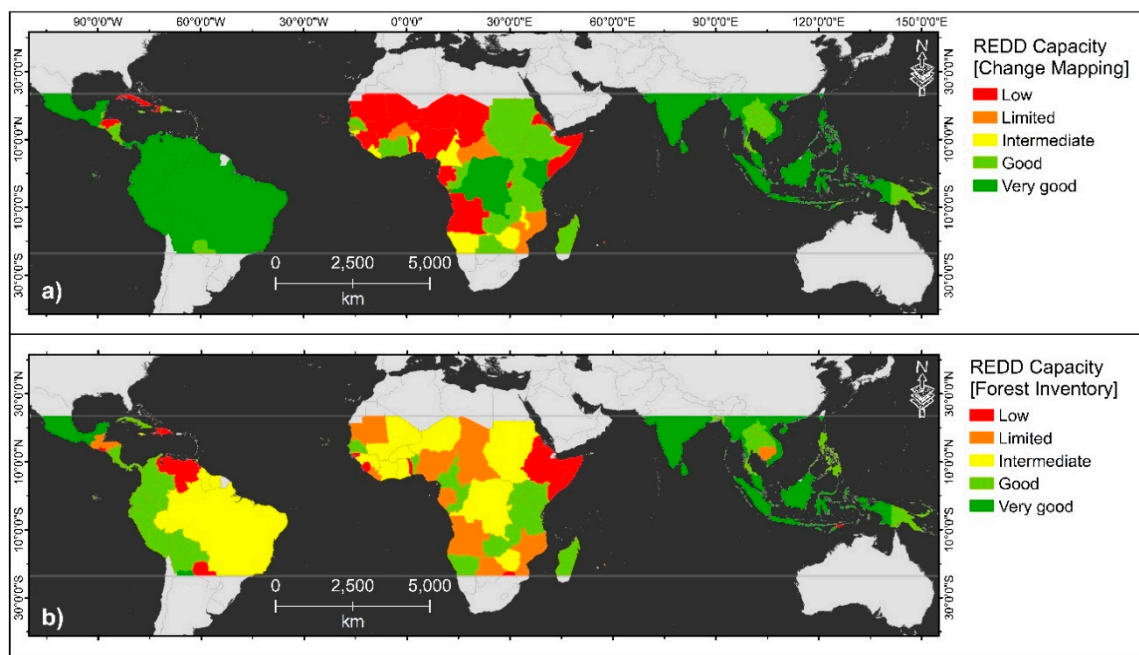

Figure 6. Capacities of the tropical countries for remote sensing based (**a**) change mapping and (**b**) forest inventory development, in the context of the REDD+ initiative [182].

7. Recent and Future Space-Borne Satellite Missions for Biomass Estimation

Global and pan-tropical studies of AGB estimate from the current satellite observations and integrated analysis of field inventories identify uncertainties and gaps in quantitative carbon stock assessments. Therefore, many space-born remote sensing missions have been launched recently, aiming at enhanced quantifications of carbon stocks across different biomes and carbon exchange associated with deforestation, degradation and LCLU changes (Figure 7).

BIOMASS, one of the Earth Explorer mission from European Space Agency, is a P-band SAR satellite remote sensing mission, which is planned to be launched by the ESA in 2022. Three primary products will be derived from the data acquired by the BIOMASS mission, including AGB, forest canopy height (upper canopy height) and forest disturbance maps. The AGB and forest height will be estimated at a 200 m spatial resolution, while forest disturbance maps will be produced at a 50 m spatial resolution [186].

A new era of forest covers dynamic monitoring will be opened with the launch of Tadem-L in 2022 by the German Aerospace Center (DLR). It is a SAR mission with two satellites operating in the L-band. The mission will provide high-resolution data to extract annual and seasonal 3-D structure, and biomass of global forests twice a year at a voxel size of $10 \times 50 \times 50$ m^3. It will provide a tree height map at 30 m and a biomass map at a 50 m spatial resolution across the globe [187].
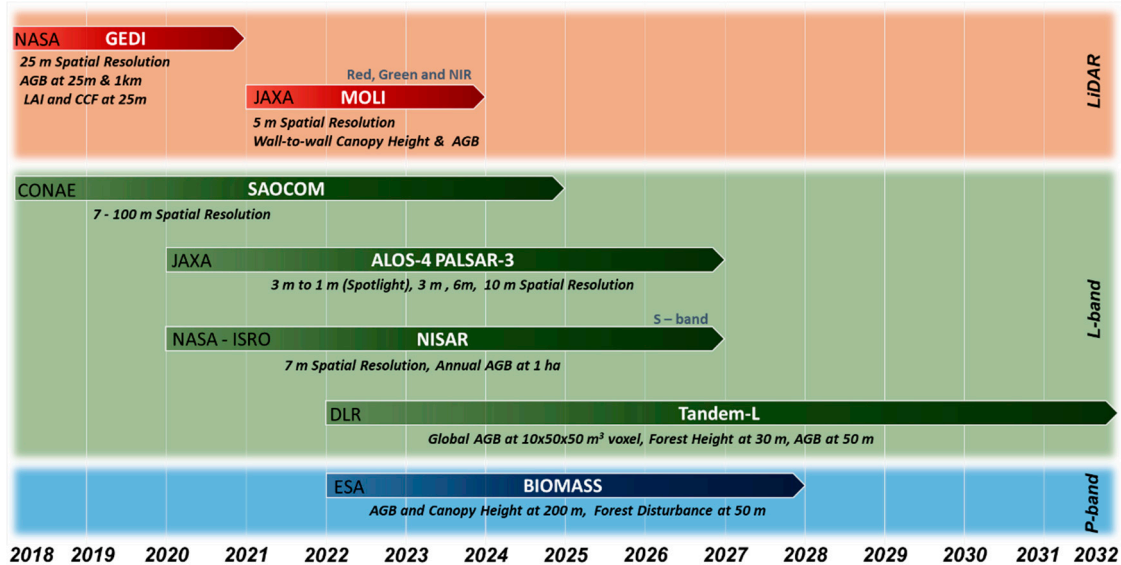
Figure 7. Satellite missions for biomass mapping—recently launched or planned to be launched in the near future.

GEDI is the first high-resolution space-borne LiDAR mission to measure the magnitude of forest biomass and vertical structure of forests between ± 51.6° latitude. It was deployed on ISS in 2018 by NASA for two years [188]. It measures surface elevation, forest canopy height and the vertical structure of the forest, which is imperative for an accurate estimate of existing forest biomass and its changes due to anthropogenic and climatic factors. The significant science products developed from GEDI include, but are not limited to, Canopy Cover Fraction (CCF), LAI, and LAI profiles at 25 m, AGB at a footprint level of 25 m, and Gridded AGB at a grid interval of 1 km [108]. The precision of the products will help to reduce uncertainties in carbon stock mapping due to deforestation, degradation and regenerating tropical forests [189].

NISAR (NASA-ISRO Synthetic Aperture Radar) is a 3-year multidisciplinary SAR mission emerged through collaboration between NASA and Indian Space Research Organization (ISRO). It is planned to be launched in 2021 and it will be hosting both S-band and L-band radars, with a spatial resolution of 7 m with a revisit time of 12 days. The mission will develop an annual global biomass product at a spatial resolution of 1 ha, which will be instrumental to monitor gains and losses in forest biomass across the tropical and other parts of the world [117,189,190]

NASA's ICESat-2 was launched in September 2019. The ATLAS onboard ICESat-2 is promised to provide altimetry observations of Earth's land surface. The primary objective of the ICESat is to measure ice sheets and land elevation. However, the data are used for the canopy height and biomass estimation; thus, the ICESat-2 generates two vegetation products ATL08 (Level-3A product) and ATL18 (Level-3B product). The ALT18 gridded land product will provide coarse resolution annual maps of canopy height and canopy cover, while ALT08 will generate the vegetation products at a 100 m spatial resolution [117]. Several studies have utilized ICESat-1's GLAS datasets to estimate pan-tropical biomass [32,105] and the new observations from ICESat-2 will help determine the changes in the AGB, as well as improving the accuracy of current carbon stock assessments [118,119].

The Argentinean SAtélite Argentino de Observación Con Microondas (SAOCOM) is an L-band SAR mission, aiming to improve global observations of forests and forest biomass change by developing a consistent time series archive. It is based on a constellation of two identical satellites SAOCOM-1A and SAOCOM-1B to provide dual-polarized Interferometric synthetic-aperture radar (InSAR) coverage with a combined revisit time of 8 days [190]. SAOCOM-1A was launched in October 2018 and SAOCOM-1B was planned to be launched in March 2020. However, its launch is delayed amid the

COVID-19 pandemic. The mission is operated and managed by Argentina's Space Agency (ASA), Buenos Aires (BA) and the Comisión Nacional de Actividades Espaciales (CONAE) [191].

The Phased Array L-band Synthetic Aperture Radar 3 (PALSAR-3) onboard Advanced Land Observing Satellite (ALOS)-4 is a JAXA's follow-on mission of PALSAR -2 onboard ALOS-2 [192]. It is planned to be launched in 2021 with a designed life of 5 years. The PALSAR-3 is designed for long-term monitoring with a 3 m spatial resolution, and it will follow the orbit of the PALSAR -2 with a 14-days temporal resolution [190,193,194]. Earlier, observations from the PALSAR-2 are extensively used to produce an annual global mosaic of SAR images at a 25 m spatial resolution, which has been used for developing numerous tropical/global biomass estimation maps [164]. The improved resolution of the PALSAR-3 will enhance the accuracy of carbon stock assessment studies in the coming decades.

The Multi-footprint Observation LiDAR and Imager (MOLI) is another biomass and canopy height mapping mission to be launched in 2022 by the JAXA. The most prominent feature of the MOLI mission is to improve the canopy height information by correcting the terrain slope error in the calculation of the canopy height using the three footprint observations. In addition to the Level 1 Waveform and multispectral image (Red, Green, NIR) products, the MOLI will provide Level 2 products of Canopy Height and Forest Biomass. The most comprehensive product of the mission will be wall-to-wall canopy height and forest biomass maps [195].

Moreover, a combination of these datasets would open new research horizons of multi-sensor data synchronization and harmonization for refined biomass measurements. For example, multi-sensor SAR time series from PALSAR-2, RADARSAT-2 and Sentinel-1 provided effective maps of selective logging in the tropical forests of Brazilian Amazon [196]. Apart from SAR time series, researchers are integrating LiDAR data from GEDI with Landsat data, that will open a new era of hindcasting forest biomass using the historic and harmonized time series of the Landsat since the late 1970s. For example, an integrated approach has been developed by combining 1607 field plots with GLAS and PALSAR-2 to estimate ABG in China at a 30 m spatial resolution [197]. Further research on integrated models will enable advanced understanding and modelling of change dynamics in the tropical forests. Besides, scientists are anticipating integration of GEDI observations with an in-orbit and near-future SAR mission to generate high-quality biomass maps. The overlapping operational lives of these satellite missions for biomass monitoring are the biggest advantage that will stimulate integration and synchronization of biomass products, for developing science-based policies to manage the tropical and/or global forest resources [23].

8. Concluding Remarks

Accurate and reliable information about the spatial distribution of tropical forest biomass is imperative for managing carbon stocks, mitigating climate change and to understand the role of the tropical forests in the global carbon budget. Remote sensing plays a pivotal role in the estimation of the extent and biomass of tropical forests. The emergence of high-performance computing has enabled upscaling of the remote-sensing-based biomass estimation methods, from localized site-specific studies to pan-tropical and global-scale AGB estimate at increasingly high spatial resolutions. In the last decade, many studies were carried to estimate pan-tropical carbon stock maps by combining field inventories with multi-source remote sensing data such as NOAA, MODIS, Landsat, SPOT, Sentinel-1 and 2, ICESat-1 and 2, and PALSAR-2. In the tropics, integration of ICESat-1's GLAS with the established data products from other satellites has generated several significant pan-tropical biomass maps at a 500 m–1 km spatial resolutions [105,156,159,162,163,186]. Global forest and non-forest mosaics at a 25 m spatial resolution have been generated from ALOS-PALSAR from 2007 to 2017 [76] and has been integrated with Sentinel-SAR images and ICESat LiDAR data to generate global AGB maps of 2017 at a 100 m spatial resolution [164]. To further enhance the accuracy and continuous development of space-based estimates and monitoring of the AGB of the forest, special biomass measurement missions have been launched and/or planned to be launched in the near future such as GEDI (LiDAR) in 2018, MOLI (Multi-footprint LiDAR) in 2022, BIOMASS (P-band SAR) in 2022, PALSAR-3 (L-band SAR)

in 2021, NISAR (S and L—band SAR) in 2021 and Tandem-L (L-band SAR) in 2022. LiDAR-based observation from the GEDI and MOLI on canopy height and vertical structure is critical in improving the accuracy using remote sensing. Overlapping operational time of these missions with different sensors (LiDAR, P, S, and L—band SAR) will open new research domains of sensors' integration and synchronizations to develop a variety of accurate products for forest biomass measurements, which will help to estimate and monitor changes in tropical forests due to deforestation, degradation, and most significantly, the recovery of the tropical forests due to abandonment. The coming decades will be revolutionary for pan-tropical biomass monitoring, due to high-performance cloud computing and the new satellite missions focusing on biomass mapping.

Conflicts of Interest: The authors declare no conflict of interest.

Appendix A

Table A1. List of abbreviation and acronyms.

Acronym	Definition
AGB	Above-Ground Biomass
ALOS	Advanced Land Observing Satellite
ALS	Airborne Laser Scanning
AMSR-E	Advanced Microwave Scanning Radiometer for EOS (AMSR-E)
ASA	Argentina's Space Agency
ASAR	Advanced Synthetic Aperture Radar
ATLAS	Advanced Topographic Altimeter System
AVHRR	Advanced Very High Resolution Radiometer
BA	Buenos Aires
BEF	Biomass Expansion Factors
BGB	Below Ground Biomass
CERES	Clouds and the Earth's Radiant Energy System
CLAS	Carnegie Landsat Analysis System
CCI	Climate Change Initiative
CGLS	Copernicus Global Land Service
CGLS-LC100	Copernicus Global Land Service – Land Cover 100
CIAT	International Center for Tropical Agriculture
CONAE	Comisión Nacional de Actividades Espaciales
CSA	Canadian Space Agency
DBH	diameter at breast height
DW	Deadwood
DLR	German Aerospace Center
EO	Earth Observation
ESA	European Space Agency
ETM+	Enhanced Thematic Mapper +
EVI	Enhanced Vegetation Index
FAO	Food and Agriculture Organization
FAPAR	Fraction of Absorbed Photosynthetically Active Radiation
FCover	Fraction of Vegetation Cover
FORMA	Forest Monitoring for Action
FOTO	Fourier-Based Textural Ordination

Table A1. *Cont.*

Acronym	Definition
FPAR	Fraction of Photosynthetically Active Radiation
FRA	Forest Resources Assessment
FREL/FRL	Forest reference emission levels and forest reference levels
FVC	Fraction of Vegetation Cover
GEDI	Global Ecosystem Dynamics Investigation
GEE	Google Earth Engine
GEO	Group on Earth Observations
GFC	Global Forest Change
GFOI	The Global Forest Observations Initiative
GFW	Global Forest Watch
GHG	Greenhouse gas
GIMMS	Global Inventory Modeling and Mapping Studies
GLAD	Global Land Analysis and Discovery
GLAS	Geoscience Laser Altimeter System
GLC	Global Land Cover
GLCF	Global Land Cover Facility
GMW	Global Mangrove Watch
GOFC-GOLD	Global Observation of Forest Cover and Land Dynamics
GORT	Geometric Optical-Radiative Transfer
GPP	Gross Primary Production
GRACE	Gravity Recovery and Climate Experiment
GSFC	Goddard Space Flight Center
Gt	Gigatons
ha	hectare
ICESat	Ice, Cloud, and Land Elevation Satellite
IFL	Intact Forest Landscapes
InSAR	Interferometric synthetic-aperture radar
IPCC	Intergovernmental Panel on Climate Change
ISRO	Indian Space Research Organization
ISS	International Space Station
IUCN	International Union for Conservation of Nature
JAXA	Japan Aerospace Exploration Agency
JERS-1	Japanese Earth Resources Satellite 1
LAD	Leaf Area Density
LAI	Leaf Area Index
LAI	Leaf Area Index
LC	Land Cover
LCLU	Land Cover Land Use
LiDAR	Light Detection and Ranging
LPDAAC	Land Processes Distributed Active Archive Center
LSP	Land Surface Phenology
MERIS	Medium Resolution Imaging Spectrometer
MMU	Minimum Mapping Unit
MODIS	Moderate Resolution Imaging Spectroradiometer
MOLI	Multi-footprint Observation LiDAR and Imager
MRV	Measuring, Reporting and Verification
NASA	National Aeronautics and Space Administration
NASG	National Administration of Surveying, Mapping and Geoinformation of China
NDVI	Normalized difference vegetation index
NEP	Net Ecosystem Production
NIR	Near Infrared
NISAR	NASA-ISRO SAR
NOAA	National Oceanic and Atmospheric Administration
NPP	Net Primary Productivity
NPP	Net Primary Productivity

Table A1. *Cont.*

Acronym	Definition
PALSAR	Phased Array type L-band Synthetic Aperture Radar
PAR	Photosynthetically Active Radiation
PgC	Petagram of Carbon
PROBA-V	Project for On-Board Autonomy—Vegetation
PTC	Percent Tree Cover
QSCAT	Quick Scatterometer
RADAR	Radio Detection and Ranging
REDD	Reducing Emissions from Deforestation and Forest Degradation
REDD+	Reducing Emissions from Deforestation and Forest Degradation, and the role of conservation, sustainable management of forests and enhancement of forest carbon stocks in developing countries
RMSE	Root Mean Square Error
SAOCOM	Argentinean SAtélite Argentino de Observación Con Microondas
SAR	Synthetic Aperture Radar
SIF	Sun-Induced Chlorophyll Fluorescence
SLC	Scan Line Corrector
SPOT	Satellite Pour l'Observation de la Terre
SRTM	shuttle radar topography mission
SVM	Support Vector Machine
TLS	Terrestrial Laser Scanning
TRMM	Tropical Rainfall Measurement Mission
TWS	Terrestrial Water Storage
UAV	Unmanned Aerial Vehicle
UMD	University of Maryland
UNFCCC	United Nations Framework Convention on Climate Change
UNSPF	United Nations Strategic Plan for Forests
USGS	United States Geological Survey
VCF	Vegetation Continuous Fields
VFP	Vertical Foliage Profile
VOP	Vegetation Optical Depth
WRI	World Resources Institute

Table A2. Description of relevant AGB mapping studies in the tropical forest.

Ecosystem Type	Study Area	Satellite/Sensor	RS Method	Biomass Scale	Accuracy	Resolution	Image Year	Field Data	Publication Year	Reference
Tropical savanna	Senegal	NOAA-7 AVHRR	Optical, Field spectrometer		$R^2 = 0.75$	1.1 km	1981	194 sites, 1 m^2	1983	[198]
Tropical forest	Brazilian Amazon	JERS-1 SAR, NOAA AVHRR	L Band SAR, Optical	0.05 ha	$R^2 = 0.30$	12.5 m	1993	15 site, 10 m by 50 m	1998	[199]
Tropical forest	Brazilian Amazon	Landsat TM	Optical Multispectral		$R^2 = 0.37$	30 m	1989 to 1995		2000	[200]
Tropical savanna	Zimbabwe and South Africa	Landsat-5, 7	Optical Multispectral		$R^2 = 0.75$ to 0.86	30 m	1998, 2000	74 sites, 120 × 120 m	2004	[201]
Tropical forest savanna	Cameroon, Uganda, Mozambique	ALOS PALSAR	Space-borne L-Band Radar		$R^2 = 0.61$ to 0.76	50 m	2007	253 plots	2009	[31]
Tropical forest	Brazilian Amazon	Landsat and LiDAR	Airborne LiDAR	0.1 ha	$R^2 = 0.80$, $R^2 = 0.84$	30 m, 1 m	1999 to 200	From Literature	2009	[33]
Tropical forest	Cambodia	ALOS PALSAR	Space-borne L-Band Radar		$R^2 = 0.64$		2010	40 plots, 30 × 30 m	2014	[202]
Tropical forest	Central Africa	Geoeye-1 and Quickbuird-2	Optical, Multispectral	100 m	$R^2 = 0.85$	Sub-meter	2012	474 samples 178 tree species	2014	[175]
Tropical forest	Southeast Asia	Google Earth™, VHR imagery	Composite RGB, Aerial Multispectral	-		50 cm, 8 cm	2012, 2013	25 plots of 1 ha	2015	[176]
Tropical forest	Inter-Continental	Pleiades images	Multispectral Textural Features	–	R = −0.42 R = −0.57 R2 = 0.47	70 cm to 1 m		328 plots of 1 ha	2017	[177]
Low biomass savanna	Senegal	ALOS-PALSAR SSM/I	RADAR and Brightness Temperature	10 tons ha^{-1}	R2 = 0.52	150 m, 100 m, 12.5 km	2006, 2009, 2010	48 sites of 50 × 50 m	2018	[203]
Seasonally dry ecosystems	Southern African	ALOS PALSAR	Space-borne L-Band Radar	≥10 MgC ha^{-1} per pixel	$R^2 = 0.57$	25 m	2007–2010	137 sites of 0.6 ha	2018	[14]
Primary and secondary tropical forest	Cambodia	Quickbird-2, LiDAR, Digital orthophotos	Optical Multispectral, ALTM 3100, Aerial Photos	Object-Based	$R^2 = 0.90$, $R^2 = 0.73$	0.61–2.44 m, 1 m, 0.5 m	2011	57 sample plots. 30 m × 30 m (38) 50 m × 50 m (19)	2018	[174]
Mixed tropical forest	Malaysia	TLS and, UAV	Integrated UAV and TLS	0.16 m^2 m^{-3}	43%	10 cm		60 × 60 m	2019	[29]
Tropical rain forest	French Guiana	RIEGL LMS-Q780 sensor	ALS	–	RMSE = 7.7	55–112 points/m2	2015	Six plots of 24,688 trees	2019	[20]
Tropical forest	Brazilian Amazon	Airborne LiDAR	ALS50-II, ALTM 3100, ALTM Orion, Harrier 68i	–	$R^2 = 0.8$	22.7 to 66.4 pts m^{-2}	2008–2017		2019	[9]
Regenerated tropical forest	Tanzania	RapidEye	Optical Multispectral	1 ha	$R^2 = 0.69$	5 m	2010, 2011	32,000 plots	2019	[173]
Tropical lowlands forest	Peru, Amazonian Basin	Planet Dove, LiDAR	Optical Multispectral, LiDAR	–	$R^2 = 0.70$	4 m	2011, 2013, 2017	equations developed by [33]	2019	[114]
Tropical forest	South America	Landsat-8, Sentinel-1, PALSAR, Airborne LiDAR	Optical Multispectral, LiDAR, SAR	–	$R^2 = 0.60$ to 0.95	30 m	2018	–	2019	[204]
Tropical dry forest	Sudanian Savanna, West Africa	Sentinel—1 and 2	Multispectral and SAR images	–	RMSE = 78.6, 60.6, 45.4	10 m	2017	218 plots 50 × 20 m	2020	[171]

Table A3. Characteristics of representative Passive satellites.

Satellite/Sensor	Spatial Resolution (m)	Revisit Time (days)	Spectral Resolution (µm)
Landsat	15–120	16	0.45–12.5 (11 bands)
SPOT	10–20	26	0..45–1.75 (5 bands)
MODIS	250–1000	0.25	0.4–14.4 (36 bands)
Quickbird	0.61–0.72	1-6	0.45–0.9 (4 bands)
Pleiades	0.5–2	1	0.47–0.94 (5 bands)
Sentinel-2	10–60	5	0.04–2.19 (12 bands)
Sentinel-3 (OLCI)	300	27	0.4–1.02 (21 bands)
CERES (TRMM)	10,000	46	0.3–100 (3 bands)
CHRIS	18-36	7	0.40–1.05 (19 bands)
RapidEye	5	5	0.44–0.85 (5 bands)
Planet Dove	4	1	0.42–0.90 (4 bands)
GeoEye	0.46–1.84	2 to 8	0.45–0.92 (4 bands)
AVHRR	1100	Twice daily	0.58–12.50 (5 bands)
MERIS (Envisat-1)	260 × 300	35	0.39 to 1.04 (15 bands)

Table A4. Characteristics of representative active satellites.

Mission	Period	Method	Specification/Products	Agency	Reference
NISAR	2021–2026	L-band	7 m spatial resolution, Annual AGB map at 1 ha	NASA-ISRO	[117]
ALOS-PALSAR	2006–2012	L-band	AGB map at 100 m	JAXA	[205]
ALOS-2 PALSAR-2	2014–2020	L-band	AGB at 250 m resolution	JAXA	[206]
ALOS-4 PALSAR-3	2021–2026	L-band	3 m × 1 m (Spotlight), 3 m × 3 m, 6 m × 6 m, 10 m × 10 m	JAXA	[194]
SAOCOM	2018–2025	L-band	7–100 m spatial resolution	CONAE	[191]
Tandem-L	2022–2032	L-band	$10 \times 50 \times 50$ m^3, Forest Height at 30 m, Forest Biomass at 50 m	DLR	[187]
BIOMASS	2022–2027	P-band	AGB at 200 m, Canopy Height at 200 m Forest Disturbance at 50 m	ESA	[186]
RADARSAT-2	2007–2020	C-Band	3–100 m Spatial resolution, AGB High-level accuracy of 0.25 ha	CSA	[207]
Sentinel-1	2014–2026	C-Band	5 m × 5 m spatial resolution, Mean AGB 70.38 ton/ha	ESA	[208]
GRACE	2002–2017	S-Band	Accuracy is sufficient to determine a change in mass equivalent to a volume of water with depth 1 cm over a radius of about 400 km. 30 day revisit.	NASA/DLR	[209]
GEDI	2018–2020	LiDAR	25 m footprint, CCF, LAI at 25 m, and AGB at 25 m and 1 km	NASA	[108]
MOLI	2022–2024	LiDAR, R, G, NIR	5 m spatial resolution Canopy Height and Forest Biomass Maps	JAXA	[195]
ICESat-1	2003–2010	LIDAR	Global forest AGB density was 210.09 Mg/ha on average	NASA/GSFC	[210]
ICESat-2	2018–2021	LIDAR	30 m spatial resolution AGB map, operates at 532 nm wavelength	NASA/GSFC	[211]

References

1. Nobre, C.A.; Sellers, P.J.; Shukla, J. Amazonian deforestation and regional climate change. *J. Clim.* **1991**, *4*, 957–988. [CrossRef]

2. Chazdon, R.L.; Broadbent, E.N.; Rozendaal, D.M.A.; Bongers, F.; Zambrano, A.M.A.; Aide, T.M.; Balvanera, P.; Becknell, J.M.; Boukili, V.; Brancalion, P.H.S.; et al. Carbon sequestration potential of second-growth forest regeneration in the Latin American tropics. *Sci. Adv.* **2016**, *2*, e1501639. [CrossRef] [PubMed]

3. Federici, S.; Tubiello, F.N.; Salvatore, M.; Jacobs, H.; Schmidhuber, J. New estimates of CO_2 forest emissions and removals: 1990–2015. *For. Ecol. Manag.* **2015**, *352*, 89–98. [CrossRef]

4. Pan, Y.; Birdsey, R.A.; Fang, J.; Houghton, R.; Kauppi, P.E.; Kurz, W.A.; Phillips, O.L.; Shvidenko, A.; Lewis, S.L.; Canadell, J.G.; et al. A large and persistent carbon sink in the world's forests. *Science* **2011**, *333*, 988–993. [CrossRef]

5. FAO. *Global Forest Resource Assessment*; FAO: Rome, Italy, 2010.

6. FAO. *Global Forest Resources Assessment 2020: Main Report*; FAO: Remote, Italy, 2020; ISBN 978-92-5-132974-0.

7. Stephens, B.B.; Gurney, K.R.; Tans, P.P.; Sweeney, C.; Peters, W.; Bruhwiler, L.; Ciais, P.; Ramonet, M.; Bousquet, P.; Nakazawa, T.; et al. Weak northern and strong tropical land carbon uptake from vertical profiles of atmospheric CO_2. *Science* **2007**, *316*, 1732–1735. [CrossRef]

8. Lewis, S.L.; Lopez-Gonzalez, G.; Sonké, B.; Affum-Baffoe, K.; Baker, T.R.; Ojo, L.O.; Phillips, O.L.; Reitsma, J.M.; White, L.; Comiskey, J.A.; et al. Increasing carbon storage in intact African tropical forests. *Nature* **2009**, *457*, 1003. [CrossRef]

9. Shao, G.; Stark, S.C.; de Almeida, D.R.A.; Smith, M.N. Towards high throughput assessment of canopy dynamics: The estimation of leaf area structure in Amazonian forests with multitemporal multi-sensor airborne lidar. *Remote Sens. Environ.* **2019**, *221*, 1–13. [CrossRef]

10. Chapin, F.S.; Matson, P.A.; Vitousek, P.M. *Principles of Terrestrial Ecosystem Ecology*; Springer: New York, NY, USA, 2011; ISBN 978-1-4419-9503-2.

11. Laurance, W.F. Gaia's Lungs: Are rainforests inhaling Earth's excess carbon dioxide? *Nat. Hist.* **1999**, *108*, 96.

12. Abbas, S.; Nichol, J.E.; Fischer, G.A. A 70-year perspective on tropical forest regeneration. *Sci. Total Environ.* **2016**, *544*, 544–552. [CrossRef]

13. Abbas, S.; Nichol, J.E.; Zhang, J.; Fischer, G.A. The accumulation of species and recovery of species composition along a 70 year succession in a tropical secondary forest. *Ecol. Indic.* **2019**, *106*, 105524. [CrossRef]

14. McNicol, I.M.; Ryan, C.M.; Mitchard, E.T.A. Carbon losses from deforestation and widespread degradation offset by extensive growth in African woodlands. *Nat. Commun.* **2018**, *9*, 3045. [CrossRef] [PubMed]

15. Kim, D.; Sexton, J.O.; Townshend, J.R. Accelerated deforestation in the humid tropics from the 1990s to the 2000s. *Geophys. Res. Lett.* **2015**, *42*, 1–7. [CrossRef] [PubMed]

16. Geist, H.J.; Lambin, E.F. Proximate causes and underlying driving forces of tropical deforestation. *Bioscience* **2002**, *52*, 143. [CrossRef]

17. Wright, S.J. Tropical forests in a changing environment. *Trends Ecol. Evol.* **2005**, *20*, 553–560. [CrossRef] [PubMed]

18. Boisvenue, C.; White, J.C. Information needs of next-generation forest carbon models: Opportunities for remote sensing science. *Remote Sens.* **2019**, *11*, 463. [CrossRef]

19. Saukkola, A.; Melkas, T.; Riekki, K.; Sirparanta, S.; Peuhkurinen, J.; Holopainen, M.; Hyyppä, J.; Vastaranta, M. Predicting forest inventory attributes using airborne laser scanning, aerial imagery, and harvester data. *Remote Sens.* **2019**, *11*, 797. [CrossRef]

20. Aubry-Kientz, M.; Dutrieux, R.; Ferraz, A.; Saatchi, S.; Hamraz, H.; Williams, J.; Coomes, D.; Piboule, A.; Vincent, G. A comparative assessment of the performance of individual tree crowns delineation algorithms from ALS data in tropical forests. *Remote Sens.* **2019**, *11*, 1086. [CrossRef]

21. Kindermann, G.E.; McCallum, I.; Fritz, S.; Obersteiner, M. A global forest growing stock, biomass and carbon map based on FAO statistics. *Silva Fenn.* **2008**, *42*, 387–396. [CrossRef]

22. MacDicken, K.; Reams, G.; de Freitas, J. Introduction to the changes in global forest resources from 1990 to 2015. *For. Ecol. Manag.* **2015**, *352*, 1–2. [CrossRef]

23. Herold, M.; Carter, S.; Avitabile, V.; Espejo, A.B.; Jonckheere, I.; Lucas, R.; McRoberts, R.E.; Næsset, E.; Nightingale, J.; Petersen, R.; et al. The role and need for space-based forest biomass-related measurements in environmental management and policy. *Surv. Geophys.* **2019**, *40*, 757–778. [CrossRef]

24. Segura, M.; Kanninen, M. Allometric models for tree volume and total aboveground biomass in a tropical humid forest in Costa Rica1. *Biotropica* **2005**, *37*, 2–8. [CrossRef]

25. Henry, M.; Picard, N.; Trotta, C.; Manlay, R.J.; Valentini, R.; Bernoux, M.; Saint-André, L. Estimating tree biomass of Sub-Saharan African forests: A review of available allometric equations. *Silva Fenn.* **2011**, *45*, 477–569. [CrossRef]

26. Popkin, G. The hunt for the world's missing carbon. *Nature* **2015**, *523*, 20–22. [CrossRef] [PubMed]

27.　Kumar, L.; Sinha, P.; Taylor, S.; Alqurashi, A.F. Review of the use of remote sensing for biomass estimation to support renewable energy generation. *J. Appl. Remote Sens.* **2015**, *9*, 097696. [CrossRef]

28.　Dube, T.; Mutanga, O.; Shoko, C.; Samuel, A.; Bangira, T. Remote sensing of aboveground forest biomass: A review. *Trop. Ecol.* **2016**, *57*, 125–132.

29.　Schneider, F.D.; Kükenbrink, D.; Schaepman, M.E.; Schimel, D.S.; Morsdorf, F. Quantifying 3D structure and occlusion in dense tropical and temperate forests using close-range LiDAR. *Agric. For. Meteorol.* **2019**, *268*, 249–257. [CrossRef]

30.　Patenaude, G.; Milne, R.; Dawson, T.P. Synthesis of remote sensing approaches for forest carbon estimation: Reporting to the Kyoto Protocol. *Environ. Sci. Policy* **2005**, *8*, 161–178. [CrossRef]

31.　Mitchard, E.T.A.; Saatchi, S.S.; Woodhouse, I.H.; Nangendo, G.; Ribeiro, N.S.; Williams, M.; Ryan, C.M.; Lewis, S.L.; Feldpausch, T.R.; Meir, P. Using satellite radar backscatter to predict above-ground woody biomass: A consistent relationship across four different African landscapes. *Geophys. Res. Lett.* **2009**, *36*, 1–6. [CrossRef]

32.　Asner, G.P.; Brodrick, P.G.; Philipson, C.; Vaughn, N.R.; Martin, R.E.; Knapp, D.E.; Heckler, J.; Evans, L.J.; Jucker, T.; Goossens, B.; et al. Mapped aboveground carbon stocks to advance forest conservation and recovery in Malaysian Borneo. *Biol. Conserv.* **2018**, *217*, 289–310. [CrossRef]

33.　Asner, G.P. Tropical forest carbon assessment: Integrating satellite and airborne mapping approaches. *Environ. Res. Lett.* **2009**, *4*, 03409. [CrossRef]

34.　Asner, G.P.; Knapp, D.E.; Martin, R.E.; Tupayachi, R.; Anderson, C.B.; Mascaro, J.; Sinca, F.; Chadwick, K.D.; Higgins, M.; Farfan, W.; et al. Targeted carbon conservation at national scales with high-resolution monitoring. *Proc. Natl. Acad. Sci. USA* **2014**, *111*, E5016–E5022. [CrossRef] [PubMed]

35.　Asner, G.P. Selective logging in the Brazilian Amazon. *Science* **2005**, *310*, 480–482. [CrossRef] [PubMed]

36.　Smith, J.E.; Heath, L.S.; Woodbury, P.B. How to estimate forest carbon for large areas from inventory data. *J. For.* **2004**, *102*, 25–31.

37.　Xiao, X.; Hagen, S.; Zhang, Q.; Keller, M.; Moore, B. Detecting leaf phenology of seasonally moist tropical forests in South America with multi-temporal MODIS images. *Remote Sens. Environ.* **2006**, *103*, 465–473. [CrossRef]

38.　Chave, J.; Andalo, C.; Brown, S.; Cairns, M.A.; Chambers, J.Q.; Eamus, D.; Fölster, H.; Fromard, F.; Higuchi, N.; Kira, T.; et al. Tree allometry and improved estimation of carbon stocks and balance in tropical forests. *Oecologia* **2005**, *145*, 87–99. [CrossRef] [PubMed]

39.　Condit, R. Methods for estimating above-ground biomass of forest and replacement vegetation in the tropics. *Cent. Trop. For. Sci. Res. Man.* **2008**, *25*, 73.

40.　Picard, N.; Saint-André, L.; Henry, M. *Manual for Building Tree Volume and Biomass Allometric Equations: From Field Measurement to Prediction*; Food and Agricultural Organization of the United Nations: Rome, Italy; Centre de Coopération Internationale en Recherche Agronomique pour le Développement: Montpeiller, France, 2012; ISBN 9789251073476.

41.　Specht, A.; West, P.W. Estimation of biomass and sequestered carbon on farm forest plantations in northern New South Wales, Australia. *Biomass Bioenergy* **2003**, *25*, 363–379. [CrossRef]

42.　Hunter, M.O.; Keller, M.; Victoria, D.; Morton, D.C. Tree height and tropical forest biomass estimation. *Biogeosciences* **2013**, *10*, 8385–8399. [CrossRef]

43.　Clark, D.B.; Kellner, J.R. Tropical forest biomass estimation and the fallacy of misplaced concreteness. *J. Veg. Sci.* **2012**, *23*, 1191–1196. [CrossRef]

44.　Lu, D.; Chen, Q.; Wang, G.; Liu, L.; Li, G.; Moran, E. A survey of remote sensing-based aboveground biomass estimation methods in forest ecosystems. *Int. J. Digit. Earth* **2016**, *9*, 63–105. [CrossRef]

45.　Masek, J.G.; Hayes, D.J.; Joseph Hughes, M.; Healey, S.P.; Turner, D.P. The role of remote sensing in process-scaling studies of managed forest ecosystems. *For. Ecol. Manag.* **2015**, *355*, 109–123. [CrossRef]

46.　Xiao, J.; Chevallier, F.; Gomez, C.; Guanter, L.; Hicke, J.A.; Huete, A.R.; Ichii, K.; Ni, W.; Pang, Y.; Rahman, A.F.; et al. Remote sensing of the terrestrial carbon cycle: A review of advances over 50 years. *Remote Sens. Environ.* **2019**, *233*, 111383. [CrossRef]

47.　Turner, D.P.; Ollinger, S.V.; Kimball, J.S. Integrating Remote Sensing and Ecosystem Process Models for Landscape- to Regional-Scale Analysis of the Carbon Cycle. *Bioscience* **2006**, *54*, 573. [CrossRef]

48. Ciais, P.; Sabine, C.; Bala, G.; Bopp, L.; Brovkin, V.; Canadell, J.; Chhabra, A.; DeFries, R.; Galloway, J.; Heimann, M.; et al. Carbon and Other Biogeochemical Cycles. In *Climate Change 2013—The Physical Science Basis*; Intergovernmental Panel on Climate Change, Ed.; Cambridge University Press: Cambridge, UK, 2013; Volume 9781107057, pp. 465–570, ISBN 9781107415324.

49. Quéré, C.; Andrew, R.; Friedlingstein, P.; Sitch, S.; Hauck, J.; Pongratz, J.; Pickers, P.; Ivar Korsbakken, J.; Peters, G.; Canadell, J.; et al. Global carbon budget 2018. *Earth Syst. Sci. Data* **2018**, *10*, 2141–2194. [CrossRef]

50. Quijas, S.; Boit, A.; Thonicke, K.; Murray-Tortarolo, G.; Mwampamba, T.; Skutsch, M.; Simoes, M.; Ascarrunz, N.; Peña-Claros, M.; Jones, L.; et al. Modelling carbon stock and carbon sequestration ecosystem services for policy design: A comprehensive approach using a dynamic vegetation model. *Ecosyst. People* **2018**, *15*, 42–60. [CrossRef]

51. Merrick, T.; Pau, S.; Jorge, M.L.S.; Bennartz, R.; Silva, T.S. Spatiotemporal patterns and phenology of tropical vegetation solar-induced chlorophyll fluorescence across Brazilian biomes using satellite observations. *Remote Sens.* **2019**, *11*, 1746. [CrossRef]

52. Jensen, J.R. *Remote Sensing of the Environment: An Earth Resource Perspective*, 2nd ed.; Pearson Education India: Bengaluru, India, 2009.

53. Harrison, S.P.; Gaillard, M.-J.; Stocker, B.D.; Vander Linden, M.; Klein Goldewijk, K.; Boles, O.; Braconnot, P.; Dawson, A.; Fluet-Chouinard, E.; Kaplan, J.O.; et al. Development and testing scenarios for implementing land use and land cover changes during the Holocene in Earth system model experiments. *Geosci. Model Dev.* **2020**, *13*, 805–824. [CrossRef]

54. Smith, M.C.; Singarayer, J.S.; Valdes, P.J.; Kaplan, J.O.; Branch, N.P. The biogeophysical climatic impacts of anthropogenic land use change during the Holocene. *Clim. Past* **2016**, *12*, 923–941. [CrossRef]

55. Buchhorn, M.; Smets, B.; Bertels, L.; Lesiv, M.; Tsendbazar, N.-E.; Herold, M.; Fritz, S. *Copernicus Global Land Service: Land Cover 100m: Epoch 2015: Globe*; OpenAIRE: Genève, Switzerland, 2019. [CrossRef]

56. Ma, W.; Domke, G.M.; Woodall, C.W.; Amato, A.W.D. Land use changes, disturbances, and their interactions on future forest aboveground biomass dynamics in the Northern US. *Forests* **2019**, *10*, 606. [CrossRef]

57. Cracknell, A.P. The exciting and totally unanticipated success of the AVHRR in applications for which it was never intended. *Adv. Space Res.* **2001**, *28*, 233–240. [CrossRef]

58. Tucker, C.; Pinzon, J.; Brown, M.; Slayback, D.; Pak, E.; Mahoney, R.; Vermote, E.; El Saleous, N. An extended AVHRR 8-km NDVI dataset compatible with MODIS and SPOT vegetation NDVI data. *Int. J. Remote Sens.* **2005**, *26*, 4485–4498. [CrossRef]

59. Minnemeyer, S.; Laestadius, L.; Sizer, N.; Saint-Laurent, C.; Potapov, P. *The Atlas of Forest Landscape Restoration Opportunities*; World Resources Institute: Washington, DC, USA. Available online: http://www.wri.org/applications/maps/flr-atlas/# (accessed on 5 August 2019).

60. Hansen, M.C.; DeFries, R.S.; Townshend, J.R.G.; Carroll, M.; Dimiceli, C.; Sohlberg, R.A. Global Percent Tree Cover at a Spatial Resolution of 500 Meters: First Results of the MODIS Vegetation Continuous Fields Algorithm. *Earth Interact.* **2003**, *7*, 1–15. [CrossRef]

61. Nguyen, T.H.; Jones, S.; Soto-Berelov, M.; Haywood, A.; Hislop, S. Landsat time-series for estimating forest aboveground biomass and its dynamics across space and time: A review. *Remote Sens.* **2019**, *12*, 98. [CrossRef]

62. GFW Global Forest Watch. Available online: https://www.globalforestwatch.org/ (accessed on 15 September 2019).

63. Hansen, M.C.; Krylov, A.; Tyukavina, A.; Potapov, P.V.; Turubanova, S.; Zutta, B.; Ifo, S.; Margono, B.; Stolle, F.; Moore, R. Humid tropical forest disturbance alerts using Landsat data. *Environ. Res. Lett.* **2016**, *11*, 034008. [CrossRef]

64. Hammer, D.; Kraft, R.; Wheeler, D. Alerts of forest disturbance from MODIS imagery. *Int. J. Appl. Earth Obs. Geoinf.* **2014**, *33*, 1–9. [CrossRef]

65. Wheeler, D.; Guzder-Williams, B.; Petersen, R.; Thau, D. Rapid MODIS-based detection of tree cover loss. *Int. J. Appl. Earth Obs. Geoinf.* **2018**, *69*, 78–87. [CrossRef]

66. Reymondin, L.; Jarvis, A.; Perez-Uribe, A.; Touval, J.; Argote, K.; Coca, A.; Rebetez, J.; Guevara, E.; Mulligan, M. Terra-i: A methodology for near real-time monitoring of habitat change at continental scales using MODIS-NDVI and TRMM. *Submitt. Remote Sens. Environ.* **2012**. Available online: http://terra-i.org/dms/docs/reports/Terra-i-Method/Terra-i%20Method.pdf (accessed on 13 September 2020).

67. Hansen, M.C.; Potapov, P.V.; Moore, R.; Hancher, M.; Turubanova, S.A.; Tyukavina, A.; Thau, D.; Stehman, S.V.; Goetz, S.J.; Loveland, T.R.; et al. High-resolution global maps of 21st-century forest cover change. *Science* **2013**, *342*, 850–853. [CrossRef]

68. Turubanova, S.; Potapov, P.V.; Tyukavina, A.; Hansen, M.C. Ongoing primary forest loss in Brazil, Democratic Republic of the Congo, and Indonesia. *Environ. Res. Lett.* **2018**, *13*, 074028. [CrossRef]

69. Buchhorn, M.; Smets, B.; Bertels, L.; Lesiv, M.; Tsendbazar, N.-E. *Copernicus Global Land Operations " 'Vegetation and Energy' "CGLOPS-1" Framework Service Contract N° 199494 (JRC), MODERATE DYNAMIC LAND COVER 100M VERSION 2*; Joint Research Centre: Ispra, Italy, 2018; ISBN 2008081120080.

70. Buchhorn, M.; Lesiv, M.; Tsendbazar, N.-E.; Herold, M.; Bertels, L.; Smets, B. Copernicus global land cover layers—Collection 2. *Remote Sens.* **2020**, *12*, 1044. [CrossRef]

71. Silva Junior, C.H.L.; Heinrich, V.H.A.; Freire, A.T.G.; Broggio, I.S.; Rosan, T.M.; Doblas, J.; Anderson, L.O.; Rousseau, G.X.; Shimabukuro, Y.E.; Silva, C.A.; et al. Benchmark maps of 33 years of secondary forest age for Brazil. *Zenodo* **2020**, *7*, 1–9.

72. Hirschmugl, M.; Deutscher, J.; Sobe, C.; Bouvet, A.; Mermoz, S.; Schardt, M. Use of SAR and optical time series for tropical forest disturbance mapping. *Remote Sens.* **2020**, *12*, 727. [CrossRef]

73. Vargas, C.; Montalban, J.; Leon, A.A. Early warning tropical forest loss alerts in Peru using Landsat. *Environ. Res. Commun.* **2019**, *1*, 121002. [CrossRef]

74. Laestadius, L.; Maginnis, S.; Minnemeyer, S.; Potapov, P.; Saint-Laurent, C.; Sizer, N. Mapping opportunities for forest landscape restoration. *Unasylva* **2011**, *62*, 1–3.

75. Bunting, P.; Rosenqvist, A.; Lucas, R.; Rebelo, L.-M.; Hilarides, L.; Thomas, N.; Hardy, A.; Itoh, T.; Shimada, M.; Finlayson, C. The global mangrove watch—A new 2010 global baseline of mangrove extent. *Remote Sens.* **2018**, *10*, 1669. [CrossRef]

76. Shimada, M.; Itoh, T.; Motooka, T.; Watanabe, M.; Shiraishi, T.; Thapa, R.; Lucas, R. New global forest/non-forest maps from ALOS PALSAR data (2007–2010). *Remote Sens. Environ.* **2014**, *155*, 13–31. [CrossRef]

77. Chapter 12—Fractional Vegetation Cover. In *Advanced Remote Sensing*, 2nd ed.; Liang, S.; Wang, J. (Eds.) Academic Press: Cambridge, MA, USA, 2020; pp. 477–510, ISBN 978-0-12-815826-5.

78. Baret, F.; Weiss, M.; Verger, A.; Smets, B. *Exploiting, Implementing Multi-Scale Agricultural Indicators Sentinels: ATBD for LAI, FAPAR and FCOVER from PROBA-V products at 300m resolution (GEOV3)*; Imagine Publishing: Bournemouth, UK, 2016.

79. Chavana-Bryant, C.; Malhi, Y.; Wu, J.; Asner, G.P.; Anastasiou, A.; Enquist, B.J.; Cosio Caravasi, E.G.; Doughty, C.E.; Saleska, S.R.; Martin, R.E.; et al. Leaf aging of Amazonian canopy trees as revealed by spectral and physiochemical measurements. *New Phytol.* **2017**, *214*, 1049–1063. [CrossRef]

80. Wu, J.; Kobayashi, H.; Stark, S.C.; Meng, R.; Guan, K.; Tran, N.N.; Gao, S.; Yang, W.; Restrepo-coupe, N.; Miura, T.; et al. Biological processes dominate seasonality of remotely sensed canopy greenness in an Amazon evergreen forest. *New. Phytol.* **2018**, *217*, 1507–1520. [CrossRef]

81. Guan, K.; Pan, M.; Li, H.; Wolf, A.; Wu, J.; Medvigy, D.; Caylor, K.K.; Sheffield, J.; Wood, E.F.; Malhi, Y.; et al. Photosynthetic seasonality of global tropical forests constrained by hydroclimate. *Nat. Geosci.* **2015**, *8*, 284–289. [CrossRef]

82. Potapov, P.; Yaroshenko, A.; Turubanova, S.; Dubinin, M.; Laestadius, L.; Thies, C.; Aksenov, D.; Egorov, A.; Yesipova, Y.; Glushkov, I.; et al. Mapping the World's Intact Forest Landscapes by Remote Sensing. *Ecol. Soc.* **2008**, *13*, 51. [CrossRef]

83. Potapov, P.; Hansen, M.C.; Laestadius, L.; Turubanova, S.; Yaroshenko, A.; Thies, C.; Smith, W.; Zhuravleva, I.; Komarova, A.; Minnemeyer, S.; et al. The last frontiers of wilderness: Tracking loss of intact forest landscapes from 2000 to 2013. *Sci. Adv.* **2017**, *3*, e1600821. [CrossRef] [PubMed]

84. Jun, C.; Ban, Y.; Li, S. Open access to Earth land-cover map. *Nature* **2014**, *514*, 434. [CrossRef] [PubMed]

85. DiMiceli, C.M.; Carroll, M.L.; Sohlberg, R.A.; Huang, C.; Hansen, M.C.; Townshend, J.R.G. *Annual Global Automated MODIS Vegetation Continuous Fields (MOD44B) at 250 m Spatial Resolution for Data Years Beginning Day 65, 2000–2010*; University of Maryland: College Park, MD, USA, 2017.

86. GeoVille Global Land Cover Dynamics 2016—2018. Sentinel-2 Time Series Analysis. Available online: https://landmonitoring.earth/portal/ (accessed on 5 August 2019).

87. Zhang, X.; Liu, L.; Yan, D. Comparisons of global land surface seasonality and phenology derived from AVHRR, MODIS, and VIIRS data. *J. Geophys. Res. Biogeosci.* **2017**, *122*, 1506–1525. [CrossRef]

88. Townshend, J.R.G.; Carroll, M.; Dimiceli, C.; Sohlberg, R.; Hansen, M.; DeFries, R. *Vegetation Continuous Fields MOD44B, 2001 Percent Tree Cover, Collection 5*; University of Maryland: College Park, MD, USA, 2011.

89. Sexton, J.O.; Song, X.P.; Feng, M.; Noojipady, P.; Anand, A.; Huang, C.; Kim, D.H.; Collins, K.M.; Channan, S.; DiMiceli, C.; et al. Global, 30-m resolution continuous fields of tree cover: Landsat-based rescaling of MODIS vegetation continuous fields with lidar-based estimates of error. *Int. J. Digit. Earth* **2013**, *6*, 427–448. [CrossRef]

90. Hansen, M.C.; Stehman, S.V.; Potapov, P.V.; Loveland, T.R.; Townshend, J.R.G.; DeFries, R.S.; Pittman, K.W.; Arunarwati, B.; Stolle, F.; Steininger, M.K.; et al. Humid tropical forest clearing from 2000 to 2005 quantified by using multitemporal and multiresolution remotely sensed data. *Proc. Natl. Acad. Sci. USA* **2008**, *105*, 9439–9444. [CrossRef] [PubMed]

91. Hansen, A.J.; Burns, P.; Ervin, J.; Goetz, S.J.; Hansen, M.; Venter, O.; Watson, J.E.M.; Jantz, P.A.; Virnig, A.L.S.; Barnett, K.; et al. A policy-driven framework for conserving the best of Earth's remaining moist tropical forests. *Nat. Ecol. Evol.* **2020**, *4*, 1377–1384. [CrossRef]

92. Harris, N.L.; Brown, S.; Hagen, S.C.; Saatchi, S.S.; Petrova, S.; Salas, W.; Hansen, M.C.; Potapov, P.V.; Lotsch, A. Baseline map of carbon emissions from deforestation in tropical regions. *Science* **2012**, *336*, 1573–1576. [CrossRef] [PubMed]

93. DeFries, R.S.; Houghton, R.A.; Hansen, M.C.; Field, C.B.; Skole, D.; Townshend, J. Carbon emissions from tropical deforestation and regrowth based on satellite observations for the 1980s and 1990s. *Proc. Natl. Acad. Sci.* **2002**, *99*, 14256–14261. [CrossRef]

94. Breda, N.J.J. Ground-based measurements of leaf area index: A review of methods, instruments and current controversies. *J. Exp. Bot.* **2003**, *54*, 2403–2417. [CrossRef]

95. Stark, S.C.; Leitold, V.; Wu, J.L.; Hunter, M.O.; de Castilho, C.V.; Costa, F.R.C.; McMahon, S.M.; Parker, G.G.; Shimabukuro, M.T.; Lefsky, M.A.; et al. Amazon forest carbon dynamics predicted by profiles of canopy leaf area and light environment. *Ecol. Lett.* **2012**, *15*, 1406–1414. [CrossRef]

96. Watson, D.J. Comparative Physiological Studies on the Growth of Field Crops: I. Variation in Net Assimilation Rate and Leaf Area between Species and Varieties, and within and between Years. *Ann. Bot.* **1947**, *11*, 41. [CrossRef]

97. Bonan, G. *Ecological Climatology: Concepts and Applications*; Cambridge University Press: Cambridge, UK, 2015.

98. Knapp, N.; Fischer, R.; Huth, A. Linking lidar and forest modeling to assess biomass estimation across scales and disturbance states. *Remote Sens. Environ.* **2018**, *205*, 199–209. [CrossRef]

99. Fisher, R.A.; Williams, M.; da Costa, A.L.; Malhi, Y.; da Costa, R.F.; Almeida, S.; Meir, P. The response of an Eastern Amazonian rain forest to drought stress: Results and modelling analyses from a throughfall exclusion experiment. *Glob. Chang. Biol.* **2007**, *13*, 2361–2378. [CrossRef]

100. Turner, D.P.; Cohen, W.B.; Kennedy, R.E.; Fassnacht, K.S.; Briggs, J.M. Relationships between leaf area index and Landsat TM Spectral vegetation indices across three temperate zone sites. *Remote Sens. Environ.* **1999**, *70*, 52–68. [CrossRef]

101. Tang, H.; Dubayah, R.; Swatantran, A.; Hofton, M.; Sheldon, S.; Clark, D.B.; Blair, B. Retrieval of vertical LAI profiles over tropical rain forests using waveform lidar at La Selva, Costa Rica. *Remote Sens. Environ.* **2012**, *124*, 242–250. [CrossRef]

102. Antonarakis, A.S.; Saatchi, S.S.; Chazdon, R.L.; Moorcroft, P.R. Using Lidar and Radar measurements to constrain predictions of forest ecosystem structure and function. *Ecol. Appl.* **2011**, *21*, 1120–1137. [CrossRef]

103. Stark, S.C.; Enquist, B.J.; Saleska, S.R.; Leitold, V.; Schietti, J.; Longo, M.; Alves, L.F.; Camargo, P.B.; Oliveira, R.C. Linking canopy leaf area and light environments with tree size distributions to explain Amazon forest demography. *Ecol. Lett.* **2015**, *18*, 636–645. [CrossRef] [PubMed]

104. De Almeida, D.R.A.; Stark, S.C.; Shao, G.; Schietti, J.; Nelson, B.W.; Silva, C.A.; Gorgens, E.B.; Valbuena, R.; Papa, D.d.A.; Brancalion, P.H.S.; et al. Optimizing the remote detection of tropical rainforest structure with airborne lidar: Leaf area profile sensitivity to pulse density and spatial sampling. *Remote Sens.* **2019**, *11*, 92. [CrossRef]

105. Baccini, A.; Goetz, S.J.; Walker, W.S.; Laporte, N.T.; Sun, M.; Sulla-Menashe, D.; Hackler, J.; Beck, P.S.A.; Dubayah, R.; Friedl, M.A.; et al. Estimated carbon dioxide emissions from tropical deforestation improved by carbon-density maps. *Nat. Clim. Chang.* **2012**, *2*, 182–185. [CrossRef]

106. Zhu, Z.; Bi, J.; Pan, Y.; Ganguly, S.; Anav, A.; Xu, L.; Samanta, A.; Piao, S.; Nemani, R.; Myneni, R. Global data sets of vegetation leaf area index (LAI)3g and fraction of photosynthetically active radiation (FPAR)3g derived from global inventory modeling and mapping studies (GIMMS) normalized difference vegetation index (NDVI3g) for the Period 1981 to 2. *Remote Sens.* **2013**, *5*, 927–948. [CrossRef]

107. Tang, H.; Dubayah, R.; Brolly, M.; Ganguly, S.; Zhang, G. Large-scale retrieval of leaf area index and vertical foliage profile from the spaceborne waveform lidar (GLAS/ICESat). *Remote Sens. Environ.* **2014**, *154*, 8–18. [CrossRef]

108. Dubayah, R.; Blair, J.B.; Goetz, S.; Fatoyinbo, L.; Hansen, M.; Healey, S.; Hofton, M.; Hurtt, G.; Kellner, J.; Luthcke, S.; et al. The Global Ecosystem Dynamics Investigation: High-resolution laser ranging of the Earth's forests and topography. *Sci. Remote Sens.* **2020**, *1*, 100002. [CrossRef]

109. Stephenson, N.L.; Das, A.J.; Condit, R.; Russo, S.E.; Baker, P.J.; Beckman, N.G.; Coomes, D.A.; Lines, E.R.; Morris, W.K.; Rüger, N.; et al. Rate of tree carbon accumulation increases continuously with tree size. *Nature* **2014**, *507*, 90–93. [CrossRef] [PubMed]

110. Sheil, D.; Eastaugh, C.S.; Vlam, M.; Zuidema, P.A.; Groenendijk, P.; van der Sleen, P.; Jay, A.; Vanclay, J. Does biomass growth increase in the largest trees? Flaws, fallacies and alternative analyses. *Funct. Ecol.* **2017**, *31*, 568–581. [CrossRef]

111. Sillett, S.C.; Van Pelt, R.; Koch, G.W.; Ambrose, A.R.; Carroll, A.L.; Antoine, M.E.; Mifsud, B.M. Increasing wood production through old age in tall trees. *For. Ecol. Manag.* **2010**, *259*, 976–994. [CrossRef]

112. Larjavaara, M.; Muller-Landau, H.C. Measuring tree height: A quantitative comparison of two common field methods in a moist tropical forest. *Methods Ecol. Evol.* **2013**, *4*, 793–801. [CrossRef]

113. Vaglio Laurin, G.; Chen, Q.; Lindsell, J.A.; Coomes, D.A.; Del Frate, F.; Guerriero, L.; Pirotti, F.; Valentini, R. Above ground biomass estimation in an African tropical forest with lidar and hyperspectral data. *ISPRS J. Photogramm. Remote Sens.* **2014**, *89*, 49–58. [CrossRef]

114. Csillik, O.; Kumar, P.; Mascaro, J.; O'Shea, T.; Asner, G.P. Monitoring tropical forest carbon stocks and emissions using Planet satellite data. *Sci. Rep.* **2019**, *9*, 17831. [CrossRef]

115. Mascaro, J.; Detto, M.; Asner, G.P.; Muller-Landau, H.C. Evaluating uncertainty in mapping forest carbon with airborne LiDAR. *Remote Sens. Environ.* **2011**, *115*, 3770–3774. [CrossRef]

116. Baccini, A.; Asner, G.P. Improving pantropical forest carbon maps with airborne LiDAR sampling. *Carbon Manag.* **2013**, *4*, 591–600. [CrossRef]

117. Duncanson, L.; Neuenschwander, A.; Hancock, S.; Thomas, N.; Fatoyinbo, T.; Simard, M.; Silva, C.A.; Armston, J.; Luthcke, S.B.; Hofton, M.; et al. Remote sensing of environment biomass estimation from simulated GEDI, ICESat-2 and NISAR across environmental gradients in Sonoma County, California. *Remote Sens. Environ.* **2020**, *242*, 111779. [CrossRef]

118. Hayashi, M.; Saigusa, N.; Oguma, H.; Yamagata, Y. Forest canopy height estimation using ICESat/GLAS data and error factor analysis in Hokkaido, Japan. *ISPRS J. Photogramm. Remote Sens.* **2013**, *81*, 12–18. [CrossRef]

119. Neuenschwander, A.; Pitts, K. The ATL08 land and vegetation product for the ICESat-2 Mission. *Remote Sens. Environ.* **2019**, *221*, 247–259. [CrossRef]

120. Potapov, P.; Li, X.; Hernandez-Serna, A.; Tyukavina, A.; Hansen, M.; Kommareddy, A.; Pickens, A.; Turubanova, S.; Tang, H.; Silva, C.; et al. Mapping and monitoring global forest canopy height through integration of GEDI and Landsat data. *Remote Sens.* **2020**. [CrossRef]

121. UMD Global Forest Canopy Height. Available online: https://glad.umd.edu/dataset/gedi/ (accessed on 24 August 2020).

122. Abbas, S.; Nichol, J.E.; Wong, M.S. Object-based, multi-sensor habitat mapping of successional age classes for effective management of a 70-year secondary forest succession. *Land Use Policy* **2018**, 1–10. [CrossRef]

123. Nichol, J.E.; Abbas, S.; Fischer, G.A. Spatial patterns of degraded tropical forest and biodiversity restoration over 70-years of succession. *Glob. Ecol. Conserv.* **2017**, *11*, 134–145. [CrossRef]

124. Moran, E.F.; Brondizio, E.; Mausel, P.; Wu, Y. Integrating amazonian vegetation, land-use, and satellite data. *Bioscience* **1994**, *44*, 329–338. [CrossRef]

125. Steininger, M.K. Tropical secondary forest regrowth in the Amazon: Age, area and change estimation with thematic mapper data. *Int. J. Remote Sens.* **1996**, *17*, 9–27. [CrossRef]

126. Sant'Anna, S.J.S.; da Costa Freitas Yanasse, C.; Hernandez Filho, P.; Mora Kuplich, T.; Vieira Dutra, L.; Frery, A.C.; Pessoa dos Santos, P. Secondary forest age mapping in Amazonia using multi-temporal Landsat/TM imagery. *Int. Geosci. Remote Sens. Symp.* **1995**, *1*, 323–325.

127. Irteza, S.M.; Nichol, J.E.; Shi, W.; Abbas, S. NDVI and fluorescence indicators of seasonal and structural changes in a tropical forest succession. *Earth Syst. Environ.* **2020**, 105524. [CrossRef]

128. Espírito-Santo, F.D.B.; Shimabukuro, Y.E.; Kuplich, T.M. Mapping forest successional stages following deforestation in Brazilian Amazonia using multi-temporal Landsat images. *Int. J. Remote Sens.* **2005**, *26*, 635–642. [CrossRef]

129. Carreiras, J.M.B.; Jones, J.; Lucas, R.M.; Shimabukuro, Y.E. Mapping major land cover types and retrieving the age of secondary forests in the Brazilian Amazon by combining single-date optical and radar remote sensing data. *Remote Sens. Environ.* **2017**, *194*, 16–32. [CrossRef]

130. Berveglieri, A.; Imai, N.N.; Tommaselli, A.M.G.; Casagrande, B.; Honkavaara, E. Successional stages and their evolution in tropical forests using multi-temporal photogrammetric surface models and superpixels. *ISPRS J. Photogramm. Remote Sens.* **2018**, *146*, 548–558. [CrossRef]

131. Zhou, T.; Shi, P.; Jia, G.; Dai, Y.; Zhao, X.; Shangguan, W.; Du, L.; Wu, H.; Luo, Y. Age-dependent forest carbon sink: Estimation via inverse modeling. *Biogeosciences* **2015**, *120*, 2473–2492. [CrossRef]

132. He, L.; Chen, J.M.; Pan, Y.; Birdsey, R.; Kattge, J. Relationships between net primary productivity and forest stand age in US forests. *Sci. J.* **2012**, *26*, 1–19.

133. Ryan, M.G.; Binkley, D.; Fownes, J.H. *Age-Related Decline in Forest Productivity: Pattern and Process*; Begon, M., Fitter, A.H.B.T.-A., Eds.; Academic Press: Cambridge, MA, USA, 1997; Volume 27, pp. 213–262, ISBN 0065-2504.

134. Giardina, F.; Konings, A.G.; Kennedy, D.; Alemohammad, S.H.; Oliveira, R.S.; Uriarte, M.; Gentine, P. Tall Amazonian forests are less sensitive to precipitation variability. *Nat. Geosci.* **2018**, *11*, 405–409. [CrossRef]

135. Law, B.E.; Turner, D.; Campbell, J.; Lefsky, M.; Guzy, M.; Sun, O.; van Tuyl, S.; Cohen, W. Carbon Fluxes Across Regions: Observational Constraints at Multiple Scales BT. In *Scaling and Uncertainty Analysis in Ecology*; Wu, J., Jones, K.B., Li, H., Loucks, O.L., Eds.; Springer Netherlands: Dordrecht, The Netherlands, 2006; pp. 167–190, ISBN 978-1-4020-4663-6.

136. Wu, J.; Albert, L.P.; Lopes, A.P.; Restrepo-Coupe, N.; Hayek, M.; Wiedemann, K.T.; Guan, K.; Stark, S.C.; Christoffersen, B.; Prohaska, N.; et al. Leaf development and demography explain photosynthetic seasonality in Amazon evergreen forests. *Science* **2016**, *351*, 972–976. [CrossRef]

137. Fischer, R.; Armstrong, A.; Shugart, H.H.; Huth, A. Simulating the impacts of reduced rainfall on carbon stocks and net ecosystem exchange in a tropical forest. *Environ. Model Softw.* **2014**, *52*, 200–206. [CrossRef]

138. Xu, L.; Saatchi, S.S.; Yang, Y.; Myneni, R.B.; Frankenberg, C.; Chowdhury, D.; Bi, J. Satellite observation of tropical forest seasonality: Spatial patterns of carbon exchange in Amazonia. *Environ. Res. Lett.* **2015**, *10*, 084005. [CrossRef]

139. Cox, P.M.; Pearson, D.; Booth, B.B.; Friedlingstein, P.; Huntingford, C.; Jones, C.D.; Luke, C.M. Sensitivity of tropical carbon to climate change constrained by carbon dioxide variability. *Nature* **2013**, *494*, 341–344. [CrossRef]

140. Bolton, D.K.; Gray, J.M.; Melaas, E.K.; Moon, M.; Eklundh, L.; Friedl, M.A. Continental-scale land surface phenology from harmonized Landsat 8 and Sentinel-2 imagery. *Remote Sens. Environ.* **2020**, *240*, 111685. [CrossRef]

141. Schimel, D.S.; House, J.I.; Hibbard, K.A.; Bousquet, P.; Ciais, P.; Peylin, P.; Braswell, B.H.; Apps, M.J.; Baker, D.; Bondeau, A.; et al. Recent patterns and mechanisms of carbon exchange by terrestrial ecosystems. *Nature* **2001**, *414*, 169–172. [CrossRef] [PubMed]

142. Potapov, P.; Laestadius, L.; Minnemeyer, S. Global Map of Potential Forest Cover. Available online: www.wri.org/forest-restoration-atlas (accessed on 9 October 2019).

143. Maxwell, S.L.; Evans, T.; Watson, J.E.M.; Morel, A.; Grantham, H.; Duncan, A.; Harris, N.; Potapov, P.; Runting, R.K.; Venter, O.; et al. Degradation and forgone removals increase the carbon impact of intact forest loss by 626%. *Sci. Adv.* **2019**, *5*, eaax2546. [CrossRef] [PubMed]

144. Houghton, R.A.; Hackler, J.L.; Daniels, R.C.; Martin Marietta Energy Systems Project. *Continental Scale Estimates of the Biotic Carbon Flux from Land Cover Change: 1850 to 1980*; Environmental Sciences Division Publication; Global Change Research Program, Environmental Sciences Division, Office of Health and Environmental Research, U.S. Department of Energy: Washington, DC, USA, 1995.

145. Achard, F.; Beuchle, R.; Mayaux, P.; Stibig, H.J.; Bodart, C.; Brink, A.; Carboni, S.; Desclée, B.; Donnay, F.; Eva, H.D.; et al. Determination of tropical deforestation rates and related carbon losses from 1990 to 2010. *Glob. Chang. Biol.* **2014**, *20*, 2540–2554. [CrossRef] [PubMed]

146. FAO. *Global Forest Resources Assessment 2020—Key Findings*; FAO: Rome, Italy, 2020; ISBN 978-92-5-132581-0.

147. Olofsson, P.; Foody, G.M.; Stehman, S.V.; Woodcock, C.E. Making better use of accuracy data in land change studies: Estimating accuracy and area and quantifying uncertainty using stratified estimation. *Remote Sens. Environ.* **2013**, *129*, 122–131. [CrossRef]

148. Keenan, R.J.; Reams, G.A.; Achard, F.; de Freitas, J.V.; Grainger, A.; Lindquist, E. Dynamics of global forest area: Results from the FAO global forest resources assessment 2015. *For. Ecol. Manag.* **2015**, *352*, 9–20. [CrossRef]

149. FAO. *Global Forest Resources Assessment 2015. How are the World's Forests Changing?* FAO: Rome, Italy, 2015.

150. Lee, D.; Skutsch, M.; Sandker, M. Challenges with measurement and accounting of the Plus in REDD+. 2018. Available online: https://www.climateandlandusealliance.org/reports/plus-in-redd/ (accessed on 13 September 2020).

151. McRoberts, R.E.; Stehman, S.V.; Liknes, G.C.; Næsset, E.; Sannier, C.; Walters, B.F. The effects of imperfect reference data on remote sensing-assisted estimators of land cover class proportions. *ISPRS J. Photogramm. Remote Sens.* **2018**, *142*, 292–300. [CrossRef]

152. Bos, A.B.; De Sy, V.; Duchelle, A.E.; Herold, M.; Martius, C.; Tsendbazar, N.-E. Global data and tools for local forest cover loss and REDD+ performance assessment: Accuracy, uncertainty, complementarity and impact. *Int. J. Appl. Earth Obs. Geoinf.* **2019**, *80*, 295–311. [CrossRef]

153. Waldron, A.; Miller, D.C.; Redding, D.; Mooers, A.; Kuhn, T.S.; Nibbelink, N.; Roberts, J.T.; Tobias, J.A.; Gittleman, J.L. Reductions in global biodiversity loss predicted from conservation spending. *Nature* **2017**, *551*, 364–367. [CrossRef]

154. Galiatsatos, N.; Donoghue, D.N.M.; Watt, P.; Bholanath, P.; Pickering, J.; Hansen, M.C.; Mahmood, A.R.J. An assessment of global forest change datasets for national forest monitoring and reporting. *Remote Sens.* **2020**, *12*, 1790. [CrossRef]

155. Requena Suarez, D.; Rozendaal, D.M.A.; De Sy, V.; Phillips, O.L.; Alvarez-Dávila, E.; Anderson-Teixeira, K.; Araujo-Murakami, A.; Arroyo, L.; Baker, T.R.; Bongers, F.; et al. Estimating aboveground net biomass change for tropical and subtropical forests: Refinement of IPCC default rates using forest plot data. *Glob. Chang. Biol.* **2019**, *15*, 3609–3624. [CrossRef] [PubMed]

156. Saatchi, S.S.; Harris, N.L.; Brown, S.; Lefsky, M.; Mitchard, E.T.A.; Salas, W.; Zutta, B.R.; Buermann, W.; Lewis, S.L.; Hagen, S.; et al. Benchmark map of forest carbon stocks in tropical regions across three continents. *Proc. Natl. Acad. Sci. USA* **2011**, *108*, 9899–9904. [CrossRef] [PubMed]

157. Tyukavina, A.; Baccini, A.; Hansen, M.C.; Potapov, P.V.; Stehman, S.V.; Houghton, R.A.; Krylov, A.M.; Turubanova, S.; Goetz, S.J. Aboveground carbon loss in natural and managed tropical forests from 2000 to 2012. *Environ. Res. Lett.* **2015**, *10*, 74002. [CrossRef]

158. Grace, J.; Mitchard, E.; Gloor, E. Perturbations in the carbon budget of the tropics. *Glob. Chang. Biol.* **2014**, *20*, 3238–3255. [CrossRef]

159. Baccini, A.; Walker, W.; Carvalho, L.; Farina, M.; Sulla-Menashe, D.; Houghton, R.A. Tropical forests are a net carbon source based on aboveground measurements of gain and loss. *Science* **2017**, *358*, 230–234. [CrossRef]

160. Hubau, W.; Lewis, S.L.; Phillips, O.L.; Affum-Baffoe, K.; Beeckman, H.; Cuní-Sanchez, A.; Daniels, A.K.; Ewango, C.E.N.; Fauset, S.; Mukinzi, J.M.; et al. Asynchronous carbon sink saturation in African and Amazonian tropical forests. *Nature* **2020**, *579*, 80–87. [CrossRef]

161. Grassi, G.; House, J.; Kurz, W.A.; Cescatti, A.; Houghton, R.A.; Peters, G.P.; Sanz, M.J.; Viñas, R.A.; Alkama, R.; Arneth, A.; et al. Reconciling global-model estimates and country reporting of anthropogenic forest CO_2 sinks. *Nat. Clim. Chang.* **2018**, *8*, 914–920. [CrossRef]

162. Mitchard, E.T.A.; Feldpausch, T.R.; Brienen, R.J.W.; Lopez-Gonzalez, G.; Monteagudo, A.; Baker, T.R.; Lewis, S.L.; Lloyd, J.; Quesada, C.A.; Gloor, M.; et al. Markedly divergent estimates of Amazon forest carbon density from ground plots and satellites. *Glob. Ecol. Biogeogr.* **2014**, *23*, 935–946. [CrossRef]

163. Avitabile, V.; Herold, M.; Heuvelink, G.B.M.; Lewis, S.L.; Phillips, O.L.; Asner, G.P.; Armston, J.; Ashton, P.S.; Banin, L.; Bayol, N.; et al. An integrated pan-tropical biomass map using multiple reference datasets. *Glob. Chang. Biol.* **2016**, *22*, 1406–1420. [CrossRef]

164. Santoro, M.; Cartus, O. *ESA Biomass Climate Change Initiative (Biomass_cci): Global Datasets of Forest Above-Ground Biomass for the Year 2017, v1*; European Space Agency, CEDA Archives: Paris, France, 2019.

165. Spawn, S.A.; Sullivan, C.C.; Lark, T.J.; Gibbs, H.K. Harmonized global maps of above and belowground biomass carbon density in the year 2010. *Sci. Data* **2020**, *7*, 112. [CrossRef]

166. Mitchard, E.T.A.; Saatchi, S.S.; Baccini, A.; Asner, G.P.; Goetz, S.J.; Harris, N.L.; Brown, S. Uncertainty in the spatial distribution of tropical forest biomass: A comparison of pan-tropical maps. *Carbon Balance Manag.* **2013**, *8*, 10. [CrossRef] [PubMed]

167. FAO. *From Reference Levels to Results Reporting: REDD+ under the United Nations Framework Convention on Climate Change, 2019 Update*; FAO: Rome, Italy, 2019; ISBN 9789251317907.

168. Mcmurray, A.; Pearson, T.; Casarim, F. *Guidance on Appliying the Monte Carlo Approach to Uncertainty Analysis in Forestry and Green House Gas Accounting*; Winrock International: Arlington, VA, USA, 2017; p. 26.

169. Santoro, M.; Beaudoin, A.; Beer, C.; Cartus, O.; Fransson, J.E.S.; Hall, R.J.; Pathe, C.; Schmullius, C.; Schepaschenko, D.; Shvidenko, A.; et al. Forest growing stock volume of the northern hemisphere: Spatially explicit estimates for 2010 derived from Envisat ASAR. *Remote Sens. Environ.* **2015**, *168*, 316–334. [CrossRef]

170. Roman-Cuesta, R.M.; Rufino, M.C.; Herold, M.; Butterbach-Bahl, K.; Rosenstock, T.S.; Herrero, M.; Ogle, S.; Li, C.; Poulter, B.; Verchot, L.; et al. Hotspots of gross emissions from the land use sector: Patterns, uncertainties, and leading emission sources for the period 2000–2005 in the tropics. *Biogeosciences* **2016**, *13*, 4253–4269. [CrossRef]

171. Forkuor, G.; Benewinde Zoungrana, J.B.; Dimobe, K.; Ouattara, B.; Vadrevu, K.P.; Tondoh, J.E. Above-ground biomass mapping in West African dryland forest using Sentinel-1 and 2 datasets—A case study. *Remote Sens. Environ.* **2020**, *236*, 111496. [CrossRef]

172. Brown, S.; Lugo, A.E. Biomass of tropical forests: A new estimate based on forest volumes. *Science* **1984**, *223*, 1290–1293. [CrossRef]

173. Gascón, L.H.; Ceccherini, G.; Haro, F.J.G.; Avitabile, V.; Eva, H. The potential of high resolution (5 m) RapidEye optical data to estimate above ground biomass at the national level over Tanzania. *Forests* **2019**, *10*, 107. [CrossRef]

174. Hirata, Y.; Furuya, N.; Saito, H.; Pak, C.; Leng, C.; Sokh, H.; Ma, V.; Kajisa, T.; Ota, T.; Mizoue, N. Object-based mapping of aboveground biomass in tropical forests using LiDAR and very-high-spatial-resolution satellite data. *Remote Sens.* **2018**, *10*, 438. [CrossRef]

175. Bastin, J.F.; Barbier, N.; Couteron, P.; Adams, B.; Shapiro, A.; Bogaert, J.; De Cannière, C. Aboveground biomass mapping of African forest mosaics using canopy texture analysis: Toward a regional approach. *Ecol. Appl.* **2014**, *24*, 1984–2001. [CrossRef]

176. Singh, M.; Evans, D.; Friess, D.A.; Tan, B.S.; Nin, C.S. Mapping above-ground biomass in a tropical forest in Cambodia using canopy textures derived from Google Earth. *Remote Sens.* **2015**, *7*, 5057–5076. [CrossRef]

177. Ploton, P.; Barbier, N.; Couteron, P.; Antin, C.M.; Ayyappan, N.; Balachandran, N.; Barathan, N.; Bastin, J.F.; Chuyong, G.; Dauby, G.; et al. Toward a general tropical forest biomass prediction model from very high resolution optical satellite images. *Remote Sens. Environ.* **2017**, *200*, 140–153. [CrossRef]

178. GFOI. *Integrating Remote-Sensing and Ground-Based Observations for Estimation of Emissions and Removals of Greenhouse Gases in Forests*; Group on Earth Observations: Geneva, Switzerland, 2013; ISBN 9789299004746.

179. GFOI. *Integration of Remote-Sensing and Ground-Based Observations for Estimation of Emissions and Removals of Greenhouse Gases in Forests: Methods and Guidance from the Global Forest Observations Initiative*; Food and Agriculture Organization: Rome, Italy, 2016.

180. Gill, M.; Jongman, R.; Luque, S.; Mora, B.; Paganini, M.; Szantoi, Z. *A Sourcebook of Methods and Procedures for Monitoring Essential Biodiversity Variables in Tropical Forests with Remote Sensing*; GOFC-GOLD Land Cover Project Office: Wageningen, The Netherlands, 2017; ISBN 2542-6729.

181. *UNESA Global Forest Goals and Targets of the UN Strategic Plan for Forests 2030*; United Nations, Department of Economics and Social Affairs: New York, NY, USA, 2019.

182. Romijn, E.; Lantican, C.B.; Herold, M.; Lindquist, E.; Ochieng, R.; Wijaya, A.; Murdiyarso, D.; Verchot, L. Assessing change in national forest monitoring capacities of 99 tropical countries. *For. Ecol. Manag.* **2015**, *352*, 109–123. [CrossRef]

183. Langner, A.; Achard, F.; Grassi, G. Can recent pan-tropical biomass maps be used to derive alternative Tier 1 values for reporting REDD+ activities under UNFCCC? *Environ. Res. Lett.* **2014**, *9*, 124008. [CrossRef]

184. Baccini, A.; Laporte, N.; Goetz, S.J.; Sun, M.; Dong, H. A first map of tropical Africa's above-ground biomass derived from satellite imagery. *Environ. Res. Lett.* **2008**, *3*, 045011. [CrossRef]

185. De Sy, V.; Herold, M.; Achard, F.; Avitabile, V.; Baccini, A.; Carter, S.; Clevers, J.G.P.W.; Lindquist, E.; Pereira, M.; Verchot, L. Tropical deforestation drivers and associated carbon emission factors derived from remote sensing data. *Environ. Res. Lett.* **2019**, *14*, 094022. [CrossRef]

186. Quegan, S.; Le Toan, T.; Chave, J.; Dall, J.; Exbrayat, J.-F.; Minh, D.H.T.; Lomas, M.; D'Alessandro, M.M.; Paillou, P.; Papathanassiou, K.; et al. The European Space Agency BIOMASS mission: Measuring forest above-ground biomass from space. *Remote Sens. Environ.* **2019**, *227*, 44–60. [CrossRef]

187. Moreira, A.; Krieger, G.; Hajnsek, I.; Papathanassiou, K.; Younis, M.; Lopez-Dekker, P.; Huber, S.; Villano, M.; Pardini, M.; Eineder, M.; et al. Tandem-L: A highly innovative bistatic sar mission for global observation of dynamic processes on the earth's surface. *IEEE Geosci. Remote Sens. Mag.* **2015**, *3*, 8–23. [CrossRef]

188. Qi, W.; Saarela, S.; Armston, J.; Ståhl, G.; Dubayah, R. Forest biomass estimation over three distinct forest types using TanDEM-X InSAR data and simulated GEDI lidar data. *Remote Sens. Environ.* **2019**, *232*, 111283. [CrossRef]

189. Patterson, P.L.; Healey, S.P.; Ståhl, G.; Saarela, S.; Holm, S.; Andersen, H.E.; Dubayah, R.O.; Duncanson, L.; Hancock, S.; Armston, J.; et al. Statistical properties of hybrid estimators proposed for GEDI—NASA's global ecosystem dynamics investigation. *Environ. Res. Lett.* **2019**, *14*, 065007. [CrossRef]

190. Yu, Y.; Saatchi, S. Sensitivity of L-band SAR backscatter to aboveground biomass of global forests. *Remote Sens.* **2016**, *8*, 522. [CrossRef]

191. Zoraya, A.; Bolaños, R. Implementing the LFM-CW MIT Radar at the Ecuadorian Space Institute: Some Results. *J. Aerosp. Technol. Manag.* **2020**, e0520. [CrossRef]

192. Motohka, T.; Kankaku, Y.; Suzuki, S.; Shimada, M. Status of the advanced land observing satellite-2 (ALOS-2) and its follow-on L-band SAR mission. *Int. Geosci. Remote Sens. Symp.* **2017**, *2017*, 2427–2429.

193. Okada, Y.; Yokota, Y.; Karasawa, A.; Matsuki, M.; Arii, M.; Nakamura, S. Hardware performance of PALSAR-3 onboard ALOS-4. *Int. Geosci. Remote Sens. Symp.* **2018**, *2018*, 4175–4176.

194. Miura, S.H.; Kankaku, Y.; Motohka, T.; Yamamoto, K.; Suzuki, S. ALOS-4 current status. In Proceedings of the Sensors, Systems, and Next-Generation Satellites XXIII, Strasbourg, France, 10 October 2019; Neeck, S.P., Kimura, T., Martimort, P., Eds.; SPIE: Bellingham, WA, USA, 2019; p. 4.

195. Murooka, J.; Mitsuhashi, R.; Sakaizawa, D.; Imai, T.; Kimura, T.; Asai, K.; Mizutani, K. Development status of MOLI (Multi-footprint Observation lidar and Imager). In Proceedings of the Sensors, Systems, and Next-Generation Satellites XXIII, Strasbourg, France, 14 October 2019; Neeck, S.P., Kimura, T., Martimort, P., Eds.; SPIE: Bellingham, WA, USA, 2019; p. 5.

196. Hethcoat, M.; Carreiras, J.; Edwards, D.; Bryant, R.; Quegan, S. Detecting tropical selective logging with sar data requires a time series approach. *bioRxiv Prepr.* **2020**, 1–33. [CrossRef]

197. Huang, H.; Liu, C.; Wang, X.; Zhou, X.; Gong, P. Integration of multi-resource remotely sensed data and allometric models for forest aboveground biomass estimation in China. *Remote Sens. Environ.* **2019**, *221*, 225–234. [CrossRef]

198. Tucker, C.; van Praet, C.; Boerwinkel, E.; Gaston, A. Satellite remote sensing of total dry matter production in the Senegalese Sahel. *Remote Sens. Environ.* **1983**, *13*, 461–474. [CrossRef]

199. Luckman, A.; Baker, J.; Honzák, M.; Lucas, R. Tropical forest biomass density estimation using JERS-1 SAR: Seasonal variation, confidence limits, and application to image mosaics. *Remote Sens. Environ.* **1998**, *63*, 126–139. [CrossRef]

200. Nelson, R.F.; Kimes, D.S.; Salas, W.A.; Routhier, M. Secondary forest age and tropical forest biomass estimation using thematic mapper imagery. *Bioscience* **2000**, *50*, 419–431. [CrossRef]

201. Samimi, C.; Kraus, T. Biomass estimation using Landsat-TM and -ETM+ a regional model: Towards for Southern Africa? *GeoJournal* **2004**, *59*, 177–187. [CrossRef]

202. Avtar, R.; Suzuki, R.; Sawada, H. Natural forest biomass estimation based on plantation information using PALSAR data. *PLoS ONE* **2014**, *9*, 1–15. [CrossRef]

203. Braun, A.; Wagner, J.; Hochschild, V. Above-ground biomass estimates based on active and passive microwave sensor imagery in low-biomass savanna ecosystems. *J. Appl. Remote Sens.* **2018**, *12*, 1. [CrossRef]

204. Fagua, J.C.; Jantz, P.; Rodriguez-Buritica, S.; Duncanson, L.; Goetz, S.J. Integrating LiDAR, multispectral and SAR data to estimate and map canopy height in tropical forests. *Remote Sens.* **2019**, *11*, 2697. [CrossRef]

205. Berninger, A.; Lohberger, S.; Stängel, M.; Siegert, F. SAR-based estimation of above-ground biomass and its changes in tropical forests of Kalimantan using L- and C-band. *Remote Sens.* **2018**, *10*, 831. [CrossRef]

206. Hayashi, M.; Motohka, T.; Sawada, Y. Aboveground biomass mapping using ALOS-2/PALSAR-2 time-series images for Borneo's forest. *IEEE J. Sel. Top. Appl. Earth Obs. Remote Sens.* **2019**, *12*, 5167–5177. [CrossRef]

207. Stelmaszczuk-Górska, M.A.; Urbazaev, M.; Schmullius, C.; Thiel, C. Estimation of above-ground biomass over boreal forests in Siberia using updated in Situ, ALOS-2 PALSAR-2, and RADARSAT-2 data. *Remote Sens.* **2018**, *10*, 1550. [CrossRef]

208. Nuthammachot, N.; Askar, A.; Stratoulias, D.; Wicaksono, P. Combined use of Sentinel-1 and Sentinel-2 data for improving above-ground biomass estimation. *Geocarto Int.* **2020**, 1–11. [CrossRef]

209. Li, B.; Rodell, M.; Kumar, S.; Beaudoing, H.K.; Getirana, A.; Zaitchik, B.F.; Goncalves, L.G.; Cossetin, C.; Bhanja, S.; Mukherjee, A.; et al. Global GRACE data assimilation for groundwater and drought monitoring: Advances and challenges. *Water Resour. Res.* **2019**, *55*, 7564–7586. [CrossRef]

210. Hu, T.; Su, Y.; Xue, B.; Liu, J.; Zhao, X.; Fang, J.; Guo, Q. Mapping global forest aboveground biomass with spaceborne LiDAR, optical imagery, and forest inventory data. *Remote Sens.* **2016**, *8*, 565. [CrossRef]

211. Narine, L.L.; Popescu, S.C.; Malambo, L. Using ICESat-2 to estimate and map forest aboveground biomass: A first example. *Remote Sens.* **2020**, *12*, 1824. [CrossRef]